Physics – Uspekhi **38** (4) 385 – 408 (1995)

PACS numbers: 71.27.+a

Hubbard model of strong correlations

Yu A Izyumov

Contents

Abstract. A state-of-the-art review is given of the investigations of the Hubbard model, which is the main model used in the theory of strongly correlated electron systems. It is shown how the main correlation effects — the metal – insulator phase transition, the appearance of localised magnetic moments, and the breakdown of the Fermi- liquid behaviour — appear in the case of strong electron correlations when $U \sim W$, where U is the Coulomb repulsion parameter and W is the band width. Different approaches to the problem, not based on perturbation theory in terms of the parameter U/W of W/U, are presented. A new method in the theory of strongly correlated systems, in which the limit of infinite number of dimensions of space, $d = \infty$, is the main feature of the review. The physical results obtained by this approach are compared with those deduced by traditional methods. An overview of the behaviour of strongly correlated systems is given for wide ranges of the model parameters U and W, and of the electron density n.

Yu A Izyumov Institute of Metal Physics, Ural Division of the Russian Academy of Sciences, ul. S Kovalevskoi 18, 620219 Ekaterinburg
Tel. (3432) 44-41-93
E-mail: mathphys@ifm.e-burg.su

Received 4 November 1994
Uspekhi Fizicheskikh Nauk **165** (4) 403 – 427 (1995)
Translated by A Tybulewicz

1. Introduction

1.1 Hamiltonian of the model

Three papers [1 – 3] appeared almost simultaneously and independently in the early seventies: they proposed a simple model of a metal, which has since become the fundamental model in the theory of strongly correlated electron systems (SCES). This model deals with a single nondegenerate energy band of electrons and a local Coulomb interaction.

The Hamiltonian of the model has just two parameters: the matrix element t of an electron jump from one site to an adjacent site in the lattice and the parameter U representing the Coloumb repulsion of two electrons at one site. In the second-quantisation representation this Hamiltonian can be written in the form

$$H = t \sum_{i,j,\sigma} C_{i\sigma}^{\dagger} C_{i\sigma} + U \sum_{i} n_{i\uparrow} n_{i\downarrow} \,. \tag{1.1}$$

Here, $C_{i\sigma}^{\dagger}$ and $C_{i\sigma}$ are the Fermi creation and annihilation operators for an electron at a site i with a spin σ, and $n_{i\sigma} = C_{i\sigma}^{\dagger} C_{i\sigma}$ is the number of electrons at this site.

The model proposed in Refs [1 – 3] has become known as the Hubbard model and it has made a fundamental

contribution to the study of the statistical mechanics of such a system, although the local form of the Coloumb interaction had been introduced earlier by Anderson for a model of an impurity in a metal [4].

It is worth mentioning also that the Hubbard model is a special case of the Shubin–Vonsovskii (Wonsowsky) model [5], put forward 30 years earlier than the model of Refs [1–3]. The Shubin–Vonsovskii model takes into account not only the Coloumb interaction at one site, but also the interaction of electrons at adjacent sites.

The simplicity and the self-sufficiency of the Hamiltonian (1.1) made the Hubbard model very popular and effective in the description of SCES, for which the Coloumb repulsion parameter U is greater than or of the order of the band width W. In the case of a simple cubic lattice, we have $W = 2zt$, where z is the number of the nearest neighbours.

The Hubbard model is the main working model in the theory of SCES. Among the real objects it best describes narrow-band transition metals and their compounds. In the case of these materials the Hubbard model is effective: it can be used to describe the magnetic and electric properties of such materials and the relationships between them.

In the Hamiltonian (1.1), written in the site representation, the Coulomb term is diagonal, whereas in the Fourier representation the kinetic term is diagonal and it corresponds to the band spectrum

$$\varepsilon_k = 2t \sum_{\alpha=1}^{d} \cos k_\alpha \,, \tag{1.2}$$

where d is the dimension of space.

The diagonality of one or another term in the Hamiltonian provides an opportunity of developing perturbation theory for two limiting cases: $U \ll W$ and $U \gg W$. They are sometimes called the limits of weak and strong coupling, respectively.

The intermediate case when

$$U \sim W \,, \tag{1.3}$$

is naturally most difficult to deal with, although physically it is the most interesting because it is in this case that the correlation effects leading to a metal–insulator phase transition are manifested most strongly, localised magnetic moments appear, and a strong coupling forms between the behaviour of charge carriers and magnetic order.

In an earlier review [6] I discussed in detail two limiting cases and I used perturbation theory in terms of the parameter U/W or W/U. In this review I shall concentrate mainly on the intermediate case, but without extrapolation from the weak or strong coupling limits. These limits will be discussed briefly before considering the case of intermediate coupling.

1.2 Weak and strong coupling limits

In the limit $U \ll W$ our system represents a Fermi liquid in which a long-range magnetic order may appear; it may be ferromagnetic (F) or of the spin density wave (SDW) type with the wave vector Q. This is the case of itinerant magnetism, without localised magnetic moments. The basic expression is that for the dynamic magnetic susceptibility considered in the random phase approximation (RPA) [7], i.e. taking account of loop diagrams

$$\chi(\boldsymbol{q}, \omega) = \frac{\chi_0(\boldsymbol{q}, \omega)}{1 - U\chi_0(\boldsymbol{q}, \omega)} \,. \tag{1.4}$$

Here

$$\chi_0(\boldsymbol{q}, \omega) = \frac{1}{N} \sum_{\boldsymbol{k}} \frac{f(\varepsilon_{\boldsymbol{k}}) - f(\varepsilon_{\boldsymbol{k}+\boldsymbol{q}})}{\omega + \varepsilon_{\boldsymbol{k}+\boldsymbol{q}} - \varepsilon_{\boldsymbol{k}} + \mathrm{i}\delta} \tag{1.5}$$

is the 'bare' (unrenormalised susceptibility of free (band) electrons and $f(\varepsilon)$ is the Fermi distribution function.

The conditions for divergence of $\chi(\boldsymbol{q}, \omega)$ at zero frequency determine the boundaries of the F phase (when $\boldsymbol{q} = 0$) and of the SDW phase (when $\boldsymbol{q} = \boldsymbol{Q}$). If nesting occurs, the divergence at $\boldsymbol{q} = \boldsymbol{Q}$ can occur for any U and the Neel temperature of the antiferromagnetic transition is

$$T_{\mathrm{N}} \approx W \exp\left(-\frac{1}{U\rho_0(\mu)}\right) \,, \tag{1.6}$$

where $\rho_0(\mu)$ is the density of states on the Fermi surface (μ is the chemical potential).

In the case of the spectrum described by expression (1.2) the nesting is complete for $\boldsymbol{Q} = (\pi, \pi, \pi)1/a$ when the band is half-filled, i.e. when $n = 1$, where n is the number of electrons per one lattice site. Deviation from the half-filled case destroys nesting and the Neel temperature T_{N} falls rapidly as μ is varied.

The boundaries of the ferromagnetic (F) and antiferromagnetic (A) phases in the (U, n) plane, which follow from the condition of divergence of the static magnetic susceptibility, are shown in Fig. 1. This diagram is identical with that which follows from the mean field approximation (MFA) [8]. In view of the electron–hole symmetry, the

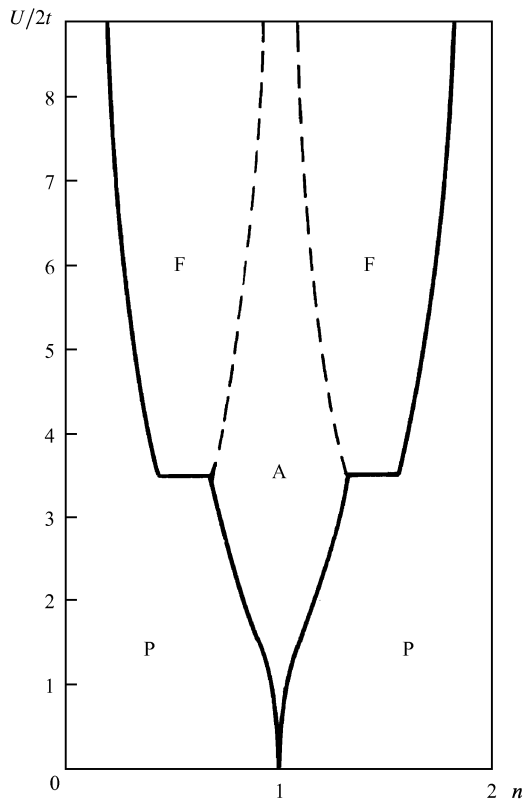

Figure 1. Magnetic phase diagram obtained in the mean field approximation [8], taking account of the existence of the paramagnetic (P), ferromagnetic (F), and antiferromagnetic (A) phases: the continuous curve represents a second-order phase transition and the dashed curve corresponds to a first-order phase transition.

pattern is symmetric relative to the point $n = 1$, so that we shall in future consider only the section $0 < n < 1$.

The problem of appearance of localised magnetic moments in the Hubbard model requires going beyond the RPA and MPA approximation.s In the weak coupling case this problem has been formulated in terms of the concept of localised spin fluctuations, which has seen rapid development in the seventies. The framework of what is known as the self-consistent theory of spin fluctuations (discussed in Moriya's monograph [9]) has made it possible to show that the magnetic susceptibility contains, like the temperature dependence described by formula (1.4), a Curie–Weiss type contribution proportional to $1/T$, which is evidence of the appearance of localised magnetic moments.

The opposite limiting case when $U \gg W$ corresponds to a strongly correlated system. When a small parameter W/U is used, it is possible to go over from the Hamiltonian (1.1) to the effective Hamiltonian in what is known as the $t-J$ model [10], which describes the motion of electrons on a lattice when there is no more than one electron at any one site and the effective exchange interaction between the nearest neighbours is described by

$$J = 2\frac{t^2}{U} . \tag{1.7}$$

Perturbation theory treatment in terms of the parameter W/U can be developed for the $t-J$ model. In this case the zeroth approximation deals with single-site atomic states, whereas the kinetic term and the effective exchange are regarded formally as perturbations [11]. In the half-filled case ($n = 1$) the Hamiltonian of the $t-J$ model reduces to the exchange Hamiltonian in the Heiesenberg model.

It follows that the Hubbard model describes itinerant magnetism in the weak coupling limit, and localised magnetism in the tight coupling limit when $n = 1$. In the intermediate range of electron densities there should be a crossover from one case to the other.

A generalised RPA can be adopted in the $t-J$ model: it involves the summation of all the loop diagrams in which the Green lines do not correspond to the electrons, as is true of the RPA approximation, but to strongly correlated electrons. The expression for the dynamic magnetic susceptibility has the structure of expression (1.4), but the 'bare' susceptibility now has two components: one of them (itinerant) is given by a formula of the (1.5) type with a correlated electron spectrum and the other depends on temperature in accordance with the $1/T$ law and takes localised magnetic moments into account.

The Curie–Weiss contribution rises steeply at some critical electron density $n_c \approx 2/3$. Therefore, near the density n_c the system crosses over from itinerant magnetism to magnetism with dual behaviour. If $n > n_c$, the system apparently is simultaneously an itinerant and localised magnetic material. Fig. 2 shows the magnetic phase diagram at $T = 0$ K obtained at the generalised RPA approximation.

Near the point $n = 1$ the Neel temperature is [12, 13]

$$T_N = \frac{1}{2}zJ - \frac{1}{4}(1-n)zt . \tag{1.8}$$

The first term represents the Curie temperature of a Heisenberg antiferromagnet and the second term takes account of the motion of holes. Since $J \ll t$, the Neel temperature T_N decreases rapidly with deviation from the case of the half-filled band.

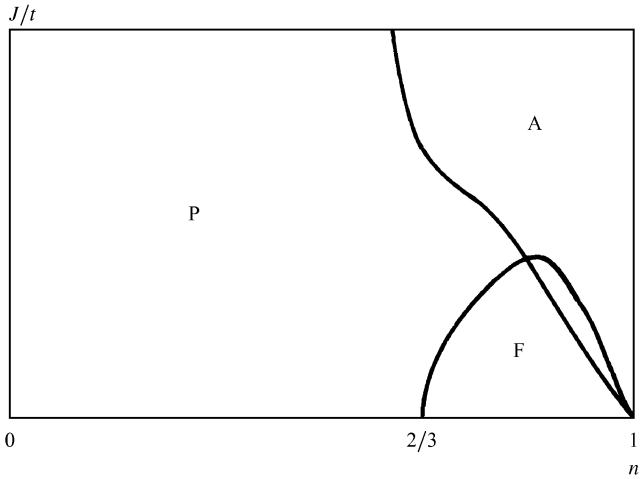

Figure 2. Magnetic phase diagram based on the $t-J$ model and the general random phase approximation [11].

1.3 Problem of the intermediate coupling

Between the two limits $U \ll W$ and $U \gg W$, when the Hubbard model describes a Fermi liquid in one case and a strongly correlated system in the other, there is a wide range of intermediate values of U in which the behaviour of the system is particularly complex. Here, both terms of the Hamiltonian (1.1) show opposite tendencies: the kinetic term corresponds to delocalisation and the Coulomb term represents localisation of the electron states, so that the electric and magnetic properties of the system depend on the fine balance between these tendencies.

A metal–insulator phase transition occurs in the intermediate range of values of U and the system goes over from itinerant magnetism to magnetism with localised magnetic moments. In the last three decades the problem has been the subject of intensive investigations (particularly in connection with the high-temperature superconductivity of copper oxide compounds), but the outlines of the solution of this problem have become clear only very recently. It is this circumstance that has provided the stimulus for writing this review.

We shall first list the methods used in the analysis of the intermediate case described by formula (1.3) when there is no formal small parameter. These methods are decoupling of the equations of motion, the mean field approximation ($d = \infty$ limit), the functional integral representation, variational methods, and the method of slave bosons and fermions.

This list should be supplemented by the numerical methods, particularly by the quantum Monte Carlo method, and the exact diagonalisation of small clusters, and also high-temperature expansions. All of them are used to monitor various types of analytic approximations.

Hubbard was the first to apply the method of decoupling of the retarded Green functions and to show that the initial electron energy band splits, because of the Coulomb repulsion at a site, into two subbands: the lower subband corre-sponds to single-particle states, and the upper to pair states.

The simplest decoupling, known in the literature as the 'Hubbard-1' [1], corresponds to the Shubin–Vonsovskii

result [5]. A more rigorous decoupling based on the 'alloy analogy' (known as the Hubbard-3 approximation [14]) leads to the Mott metal–insulator phase transition [15] precisely at the critical value of the parameter $U_c \sim W$.

The Hubbard approximations [1, 14] are not fully controlled and have serious shortcomings, discussed in detail in Section 3 below. However, from the formal point of view these approximations are very fruitful and they should be regarded as an interpolation between the limits of weak and strong coupling or between two types of electron states in the lattice: band and atomic.

An important breakthrough in the SCES theory had been made recently by Metzner and Vollhardt [16] by considering the limit of infinite number of dimensions in space: $d = \infty$. They found that many approximations used earlier heuristically in the SCES theory and in tackling other problems in many-body theories are exact in the limit $d = \infty$. This is true of the well-known coherent potential approximation (CPA), which is an integral part of the approximate methods used in the Hubbard model and is based on the representation of the partition function by functional integrals [17, 18].

Moreover, the familiar Gutzwiller approximation [19] used in the variational approach is also exact in the limit $d = \infty$. It has been found that in the same limit $d = \infty$ the Hubbard model is equivalent to certain auxiliary one-impurity Anderson models and this correspondence underlies the mean field approximation used in the Hubbard model. This approximation provides a correct description of the metal–insulator transition and of breakdown of the Fermi liquid behaviour when the parameter U increases.

The limit of infinite-dimensional space, $d = \infty$, is central in the approach used in the present review. I shall also consider systematically all other approaches mentioned above. I shall base this discussion on the methodological principle, because it is very important to analyse the capabilities of each approach within the limits of its validity (none of the approaches is universal) and the relationship between the various phenomena such as the states of the electron spectrum and the magnetic ordering. I shall leave to Section 7 an attempt to outline a general physical picture of the behaviour of the Hubbard model on the basis of the information obtained by various methods.

2. Decoupling of the equations of motion

2.1 Equations of motion for retarded Green functions

In his very first investigations of the correlation effects, Hubbard used the method of two-time Green functions [20, 21], which is particularly convenient when the interaction between the particles is strong and there is no small parameter associated with this interaction ($U \sim W$). In this situation the infinite chain of equations for the initial Green function is frequently decoupled and the many-particle Green functions (or correlation functions) are reduced to simpler forms. Such decoupling is usually of heuristic nature and is supported by the reasonableness of the physical results.

Following Hubbard's classical treatments [1, 4], let us consider the one-particle retarded Green function of electrons

$$G_{ij}^{\sigma}(\omega) = \langle\langle C_{i\sigma} | C_{j\sigma}^{\dagger} \rangle\rangle_{\omega} \,. \tag{2.1}$$

The standard notation [21] is used here and later: the symbol $\langle\langle A | B \rangle\rangle$ is the two-time Green function constructed from two operators A and B, which depend on times t and t', respectively; the index ω corresponds to the Fourier components in terms of the variable $t - t'$.

Differentiation with respect to time t gives a chain of equations for the Fourier transform of the function $\langle\langle A | B \rangle\rangle$ and the first of these equations is

$$\omega \langle\langle A | B \rangle\rangle_{\omega} = \langle [A, B] \rangle_{\eta} + \langle\langle [A, H] | B \rangle\rangle_{\omega} \,. \tag{2.2}$$

Here $[A, B]_{\eta} = AB - \eta BA$ (where η can be equal to 1 or -1; $\langle \ldots \rangle$ is the symbol for statistical averaging with the Hamiltonian H; $A, H]$ is the commutator of A and H.

The procedure of decoupling a chain of equations must be based on some physical considerations. Hubbard has proposed that in the $U \sim W$ case one should take into account exactly the electron correlations at one site and to treat the correlations at different sites in the single-site approximation.

Another methodological aspect involves the use of the 'alloy analogy' in which one considers the lattice motion of a given electron from one site to another, which may be either occupied by another electron (but with the opposite spin!) or may be free, as the motion of an electron in a disordered alloy consisting of two types of atoms a and b. The probability of occupancy n^{a} and n^{b} for atoms of a given kind is introduced and the electron Green function is averaged over all the configurations.

In the Hubbard model it is necessary to introduce similar quantities:

$$n_{i\sigma}^{\alpha} = \begin{cases} n_{i\sigma}\,, & \alpha = 1\,, \\ 1 - n_{i\sigma}\,, & \alpha = 2\,, \end{cases} \tag{2.3}$$

where $n_{i\sigma}$ is the electron number operator for a site i with a spin σ. These quantities satisfy the conditions

$$n_{i\sigma}^{\alpha} n_{i\sigma}^{\beta} = \delta_{\alpha\beta} n_{i\sigma}^{\alpha}\,, \qquad \sum_{\alpha} n_{i\sigma}^{\alpha} = 1 \,. \tag{2.4}$$

The second relationship in formula (2.4) can be used to rewrite the definition of the Green function (2.1) in the form [14]

$$G_{ij}^{\sigma}(\omega) = \sum_{\alpha} \langle\langle n_{i,-\sigma}^{\alpha} C_{i\sigma} | C_{j\sigma}^{\dagger} \rangle\rangle_{\omega} \,. \tag{2.5}$$

We can see here the advantages of the site representation in the case of the problem of a lattice with a local interaction: this representation makes it possible to include directly the correlation of electrons with opposite spins at a site.

The equation of motion for each of the components in the function (2.5) is

$$\begin{aligned} &(\omega - \varepsilon_{\alpha}) \langle\langle n_{i,-\sigma}^{\alpha} C_{i\sigma} | C_{j\sigma}^{\dagger} \rangle\rangle_{\omega} \\ &\quad = n_{-\sigma}^{\alpha} \Big\{ \delta_{ij} + \sum_{k} t_{ik} \langle\langle C_{k\sigma} | C_{j\sigma}^{\dagger} \rangle\rangle_{\omega} \Big\} \\ &\quad + \sum_{k} t_{ik} \langle\langle (n_{i,-\sigma}^{\alpha} - n_{-\sigma}^{\alpha}) C_{i\sigma} | C_{j\sigma}^{\dagger} \rangle\rangle_{\omega} + \xi_{\alpha} \sum_{k} t_{ik} \\ &\quad \times \Big\{ \langle\langle C_{i-\sigma}^{\dagger} C_{k-\sigma} C_{i\sigma} | C_{j\sigma}^{\dagger} \rangle\rangle_{\omega} + \langle\langle C_{k-\sigma}^{\dagger} C_{i-\sigma} C_{i\sigma} | C_{j\sigma}^{\dagger} \rangle\rangle_{\omega} \Big\} \,. \end{aligned} \tag{2.6}$$

Here ε_{α} is the energy of an electron at one atom for two states, i.e. one when the atom has an electron (with the opposite spin) and the other when the atom has a free level:

$$\varepsilon_+ = U - \mu, \quad \varepsilon_- = -\mu \tag{2.7}$$

(these energies are measured from the chemical potential μ) and $\xi_\pm = \pm 1$.

The quantity n_σ^α in Eqn (2.6) is the average value of an electron at a site i, i.e. $\langle n_{-\sigma}^\alpha \rangle$. It is assumed that $\langle n_{-\sigma}^\alpha \rangle$ is independent of i, i.e. that the paramagnetic or ferromagnetic states are considered. The last two terms in Eqn (2.6) take account of the correlation at different sites.

At this stage Eqn (2.6) is exact. The two approximations are used widely and they are known in the literature as Hubbard-1 and Hubbard-3 (the models are numbered in the same way as the first and third papers [1, 14] in Hubbard's series).

2.2 Hubbard-1 approximation

The last two terms are dropped from Eqn (2.6) in this approximation, i.e. the correlations at different sites are ignored. This gives the following closed equation:

$$\langle\langle C_{i\sigma} | C_{j\sigma}^\dagger \rangle\rangle_\omega = \frac{1}{F_0^\sigma(\omega)} \left\{ \delta_{ij} + \sum_k t_{ik} \langle\langle C_{k\sigma} | C_{j\sigma}^\dagger \rangle\rangle_\omega \right\},$$

which after Fourier transformation has the solution

$$G_0^\sigma(\boldsymbol{k}, \omega) = \frac{1}{F_0^\sigma(\omega) - \varepsilon_k}, \tag{2.8}$$

where $F_0^\sigma(\omega)$ is given by the relationship

$$\frac{1}{F_0^\sigma(\omega)} = \sum_\alpha \frac{n_{-\sigma}^\alpha}{\omega - \varepsilon_\alpha} = \frac{1 - n_{-\sigma}}{\omega + \mu} + \frac{n_{-\sigma}}{\omega - U + \mu}. \tag{2.9}$$

The quantity ε_k in the solution (2.8) describes the hopping of an electron from one lattice site to another and $F_0^\sigma(\omega)$ takes account of the resonant properties of the atom. It follows from the definition (2.9) that the first term describes a resonance at a free atomic level and the second term represents a resonance at an atom which already contains an electron.

The relative weight of the contributions of these resonances is given by the probability n_σ of finding an electron at a given site. The Hubbard-I approximation corresponding to the solution (2.8) thus describes the motion of an electron on a lattice characterised by some average distribution of all the other electrons at its sites. This is an approximation of the mean field type.

The solution (2.8) can be rewritten in the form

$$G_0^\sigma(\boldsymbol{k}, \omega) = \frac{P_{1\sigma}(\boldsymbol{k})}{\omega - E_{1\sigma}(\boldsymbol{k}) + \mu} + \frac{P_{2\sigma}(\boldsymbol{k})}{\omega - E_{2\sigma}(\boldsymbol{k}) + \mu}, \tag{2.10}$$

where

$$E_{1,2\sigma}(\boldsymbol{k}) = \frac{1}{2}\left[\varepsilon_{\boldsymbol{k}} + U \mp \sqrt{\varepsilon_{\boldsymbol{k}}^2 - 2\varepsilon_{\boldsymbol{k}} U(1 - 2n_{-\sigma}) + U^2}\right], \tag{2.11}$$

$$P_{1,2\sigma}(\boldsymbol{k}) = \frac{1}{2}\left[1 \mp \frac{\varepsilon_{\boldsymbol{k}} - U(1 - 2n_{-\sigma})}{\sqrt{\varepsilon_{\boldsymbol{k}}^2 - 2\varepsilon_{\boldsymbol{k}} U(1 - 2n_{-\sigma}) + U^2}}\right], \tag{2.12}$$

i.e. when the Hubbard-1 approximation yields two branches of the spectrum (Hubbard subbands) split by an amount of the order of U. This splitting remains finite for any Coulomb interaction, no matter how weak, and this is an important shortcoming of the Hubbard-1 approximation. In fact, for a half-filled band in the paramagnetic state the density of states

$$\rho(\omega) = -\frac{1}{\pi N} \operatorname{Im} \sum_k G(\boldsymbol{k}, \omega) \tag{2.13}$$

is a symmetric function. Both subbands are shifted symmetrically relative to the Fermi level and, therefore, the system is an insulator. It remains an insulator for any value of the parameter U. Therefore, the Hubbard-1 approximation does not describe the metal–insulator phase transition. These shortcomings are removed in the approximation considered below.

2.3 Hubbard-3 approximation

The correlation effects at different sites are described by the last two terms of Eqn (2.6), but these terms play a somewhat different role. In accordance with Hubbard's terminology, they represent the corrections due to the scattering by spin disorder and due to resonance broadening, caused by the motion of electrons with spin σ [represented by terms with ξ_α in Eqn (2.6)].

We shall first consider the scattering correction. We shall use again the second equality in formula (2.4). This gives the relationship

$$\langle\langle (n_{i,-\sigma}^\alpha - n_{-\sigma}^\alpha) C_{k\sigma} | C_{j\sigma}^\dagger \rangle\rangle_\omega = \sum_\beta \langle\langle (n_{i,-\sigma}^\alpha - n_{-\sigma}^\alpha)\, n_{k,-\sigma}^\beta C_{k\sigma} | C_{j\sigma}^\dagger \rangle\rangle_\omega,$$

which makes it possible to include the single-site correlations. We shall now write down the equations for the Green function on the right-hand side of the above relationship. If $i \neq k$, this relationship can yield an expression in terms of the Green function, containing the single-band correlations:

$$\langle\langle (n_{i,-\sigma}^\alpha - n_{-\sigma}^\alpha) C_{k\sigma} | C_{j\sigma}^\dagger \rangle\rangle_\omega = \sum_l \left(G_{kl}^{0\sigma} - \frac{G_{ki}^{0\sigma} G_{il}^{0\sigma}}{G_{ii}^{0\sigma}} \right) \times t_{li} \langle\langle (n_{i,-\sigma}^\alpha - n_{-\sigma}^\alpha) C_{i\sigma} | C_{j\sigma}^\dagger \rangle\rangle_\omega. \tag{2.14}$$

Here,

$$G_{ij}^0(\omega) = \frac{1}{N} \sum_{\boldsymbol{k}} \frac{\exp\left[\mathrm{i}\boldsymbol{k} \cdot (\boldsymbol{R}_i - \boldsymbol{R}_j)\right]}{F_0^\sigma(\omega) - \varepsilon_{\boldsymbol{k}}}$$

is the Green function used in the site approximation in Hubbard-1.

The scattering correction in Eqn (2.6), found with the aid of expression (2.14), yields the term

$$\lambda_\sigma'(\omega) \langle\langle (n_{i,-\sigma}^\alpha - n_{-\sigma}^\alpha) C_{i\sigma} | C_{j\sigma}^\dagger \rangle\rangle_\omega,$$

where

$$\lambda_\sigma'(\omega) = \sum_{k,l} t_{ik} \left(G_{kl}^{0\sigma} - \frac{G_{ki}^{0\sigma} G_{il}^{0\sigma}}{G_{ii}^{0\sigma}} \right) = F_\sigma^0(\omega) - \frac{1}{G_{ii}^{0\sigma}(\omega)}. \tag{2.15}$$

We can treat similarly also the last (resonance) contribution to Eqn (2.6). The result is a closed equation, which can be written in the form

$$\begin{aligned}(\omega - \varepsilon_\alpha) \langle\langle n_{i,-\sigma}^\alpha C_{i\sigma} | C_{j\sigma}^\dagger \rangle\rangle_\omega &= n_{-\sigma}^\alpha \left\{ \delta_{ij} + \sum_k t_{ik} \langle\langle C_{k\sigma} | C_{j\sigma}^\dagger \rangle\rangle_\omega \right\} \\ &- \xi_\alpha n_{-\sigma}^+ \Omega_\sigma(\omega) \langle\langle n_{i,-\sigma}^- C_{i\sigma} | C_{j\sigma}^\dagger \rangle\rangle_\omega \\ &+ \xi_\alpha n_{-\sigma}^- \Omega_\sigma(\omega) \langle\langle n_{i,-\sigma}^+ C_{i\sigma} | C_{j\sigma}^\dagger \rangle\rangle_\omega.\end{aligned} \tag{2.16}$$

The quantity $\Omega_\sigma(\omega)$, introduced above, has three components:

$$\Omega_\sigma(\omega) = \Omega'_\sigma(\omega) + \Omega'_{-\sigma}(\omega) + \Omega''_{-\sigma}(\omega) \,, \tag{2.17}$$

where

$$\Omega''_{-\sigma}(\omega) = -\Omega'_{-\sigma}(\varepsilon_+ + \varepsilon_- - \omega) \,. \tag{2.18}$$

The quantity $\Omega'_\sigma(\omega)$ is obtained from the component $\lambda'_\sigma(\omega)$, defined by formula (2.15), if we make the substitutions

$$F_0^\sigma \to F^\sigma \,, \quad G_{ii}^0 \to G_{ii} \,, \tag{2.19}$$

where F^σ and G_{ii} are found in a self-consistent manner by solving Eqn (2.16). We then have

$$\Omega'_{-\sigma}(\omega) = F^\sigma(\omega) - \frac{1}{G_{ii}^\sigma(\omega)} \,, \tag{2.20}$$

where

$$G_{ii}^\sigma(\omega) = \frac{1}{N}\sum_{\boldsymbol{k}} G(\boldsymbol{k},\omega) \,, \tag{2.21}$$

$$G^\sigma(\boldsymbol{k},\omega) = \frac{1}{F^\sigma(\omega) - \varepsilon_{\boldsymbol{k}}} \,, \tag{2.22}$$

$$\frac{1}{F^\sigma(\omega)} = \frac{\omega - (n_{-\sigma}^+\varepsilon_- + n_{-\sigma}^-\varepsilon_+) - \Omega_\sigma(\omega)}{(\omega - \varepsilon_- - n_{-\sigma}^+\Omega_\sigma)(\omega - \varepsilon_+ - n_{-\sigma}^-\Omega_\sigma) - n_{-\sigma}^+ n_{-\sigma}^- \Omega_\sigma^2} \,. \tag{2.23}$$

Expressions (2.22) and (2.23) represent the Hubbard-3 approximation. The function Ω_σ is found by a self-consistent procedure from expressions (2.17)–(2.21).

The self-consistent procedure, involving the substitution described by formula (2.19), has not been even partly justified, but it does lead to the metal–insulator phase transition. We shall consider later the physical consequences which follow from the Hubbard-3 approximation, but at this stage we shall reformulate our equations.

We shall write down the main expression (2.22) for the Green function in its usual form by introducing the self-energy part $\Sigma(\omega)$ with the aid of the following relationship (we shall omit the spin index of all the quantities and thus consider the paramagnetic phase):

$$F(\omega) \equiv \omega - \Sigma(\omega) + \mu \,. \tag{2.24}$$

Then expression (2.20)–(2.22) can be represented in the form

$$G_{ii}^\sigma(\omega) = \frac{1}{N}\sum_{\boldsymbol{k}} \frac{1}{\omega - \varepsilon_{\boldsymbol{k}} - \Sigma(\omega) + \mu} \,, \tag{2.25}$$

$$\Sigma(\omega) = \mathcal{G}^{-1}(\omega) - G_{ii}^{-1}(\omega) \,. \tag{2.26}$$

The above expression contains a formally introduced auxiliary function

$$\mathcal{G}^{-1}(\omega) = \frac{1}{\omega - \Omega'(\omega) + \mu} \,, \tag{2.27}$$

which is governed entirely by the quantity $\Omega'(\omega)$. This quantity is found from the system of self-consistent equations (2.20) in which use is made of expressions (2.23) and (2.17).

The equations for the Hubbard model in the limit of infinite dimensionality of space have the same form as Eqns (2.25) and (2.26). The Hubbard-3 approximation leads to the function $\Sigma(\omega)$, independent of the wave vector, which in the site space corresponds to the local form $\Sigma_{ij} = \delta_{ij}\Sigma$. This is strictly true in the limit $d = \infty$ (see Section 3). The nature of the function (2.27) is the same as that of the Green function of an auxiliary single-site problem characterised by the self-energy $\Omega'(\omega)$. In the Hubbard-3 approximation the self-energy $\Omega'(\omega)$ is found from the above self-consistent equations.

We shall show later, however, that the complete system of equations (2.25)–(2.27), in which the definitions (2.23) and (2.20) are used, does not correspond fully to the exact equations for the model in the limit $d = \infty$, although it has many features in common. Since the $d = \infty$ limit corresponds approximately to the mean field approach, we can say that the Hubbard-3 theory [14] is simply a variant of a theory of the mean field type. We shall see later how reliable is the Hubbard-3 theory [14] and what are its shortcomings.

Hubbard investigated a special case with one electron per atom, i.e. the half-filled case ($n = 1$). In the paramagnetic phase characterised by $n_\uparrow = n_\downarrow = n/2$ and when the model density of states is

$$\rho_0(\omega) = \frac{1}{\pi W}\sqrt{1 - \left(\frac{\omega}{W/2}\right)^2} \,, \quad |\omega| < \frac{W}{2} \,, \tag{2.28}$$

the main equations (2.20)–(2.23) can be solved analytically. In particular, the quantities $G_{ii}(\omega)$ and $\Omega'(\omega)$ can be found in terms of $F(\omega)$:

$$G_{ii}(\omega) = \frac{1}{\pi W^2}\left[F(\omega) - \sqrt{F(\omega) - \left(\frac{W}{2}\right)^2}\,\right] \,. \tag{2.29}$$

Substituting the solution (2.29) in Eqn (2.20) and then combining it with Eqn (2.23), we obtain a cubic equation for the quantity $F(\omega)$. Depending on the value of the parameter W/U, there are ranges of ω where the solution for $F(\omega)$ has either three real roots or one real and two complex. In the former case the quasiparticle density of states $\rho(\omega)$ vanishes, but in the second case it is finite (Fig. 3).

Numerical calculations show that at the critical value

$$\left(\frac{W}{U}\right)_c = 1.15 \tag{2.30}$$

there is a change in the topology of the $\rho(\omega)$ curve at the Fermi level $\mu = U/2$, which corresponds to the metal–insulator transition. This transition is continuous. In the

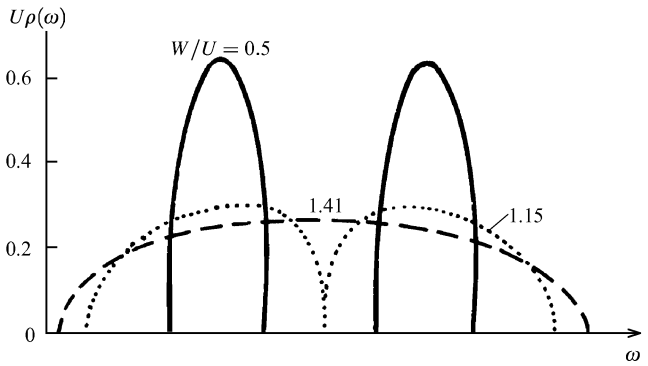

Figure 3. Quasiparticle density of states calculated for different values of W/U when $n = 1$ [14].

metal phase the density of states at the Fermi level obeys the law

$$U\rho(\omega) \propto \left[\left(\frac{W}{U}\right)_c - \frac{W}{U}\right]^{3/2} . \tag{2.31}$$

It therefore follows that the Hubbard-3 approximation describes the phase transition from the metal to the insulator phase, predicted by Mott [15] when the Coulomb parameter has the value $U \sim W$, which undoubtedly is the major success of this approximation. However, certain difficulties are encountered in the Hubbard-3 and similar approximations [22–24]. They are related primarily to the breakdown of the fundamental properties of the Green function [25, 26].

2.4 Analysis of the simplest approximations

The correlation-induced band splitting, predicted even by the Hubbard-1 approximation, is a very interesting result, but it is unsatisfactory from the physical point of view, because such splitting occurs for any value of U, no matter how small. Therefore, this splitting does not provide a correct transition of the Fermi-liquid theory. Other shortcomings of this approximation have been reported later (breakdown of the sum rule and dynamic instability of the quasiparticle spectrum), so that it cannot be used to calculate the thermodynamic properties of the model. The Hubbard-1 approximation is thermodynamically unstable even near the half-filled configuration. Another shortcoming is the absence of quasiparticle decay.

The Hubbard-3 approximation is physically more attractive, because it leads to the band splitting only if U is sufficiently large. Moreover, quasiparticles decay. However, we can easily see that the decay is proportional to $\operatorname{Im} G_{ii}$ and, therefore, it is finite over the whole spectrum, including the Fermi level. This means that there is no jump in the distribution of the particle number on the 'Fermi surface', i.e. there is no Fermi surface.

In other words, the Hubbard-3 approximation describes non-Fermi-liquid behaviour of the system throughout the full range of the parameters. Therefore, as in Hubbard-1, there is no going to the limit when the values of U are small. It is also found that the theory of the Hubbard-3 approximation is not fully self-consistent and the results of a determination of the thermodynamic quantities depend on the calculation method [27, 28].

The analytic properties of the Green functions are different for Hubbard-1 and Hubbard-3. In fact, in the former case the Green function has poles on the real axis (corresponding to two Hubbard subbands), whereas in the latter case (Hubbard-3) there is a cut on this axis. The analytic behaviour of the retarded Green function has not yet been proved for the upper half-plane, but it can be postulated because the approximation itself is analogous to the coherent potential approximation in the theory of binary alloys and the Green function in this theory is analytic [29].

In any case, the published investigations of the Hubbard-3 approximation, including numerical calculations, have not revealed breakdown of the analytic properties. However, in a related problem of the $s-d$ model, in which the technique of decoupling of the Green functions is used in the spirit of the self-consistent Hubbard approximation, it has been found [27, 28] that such breakdown may occur for some types of self-consistency which are simpler than those used in the Hubbard-3 approximation. In particular, a cut may appear on the imaginary axis in the upper half-plane and this unavoidably leads to breakdown of the sum rule. Therefore, caution is necessary when self-consistent procedures are used in the technique of decoupling of the Green functions.

The structure of the density of states $\rho(\omega)$ corresponding to the Hubbard-3 approximation consists of just two smoothed-out peaks free of the Van Hove singularities. This occurs because Hubbard-3 ignores the corrections that depend on the Fermi distribution functions and can thus result in the failure of the rigid band pattern, i.e. it may lead to a singularity of $\rho(\omega)$ of, for example, Kondo effect type. In Section 3 we shall show that a consistent mean field theory (i.e. the limit $d=\infty$) makes it possible to take account of such effects and then the density of states $\rho(\omega)$ has a more complex structure which reflects Kondo singularities on the Fermi surface.

3. Limit of infinite-dimensional space

3.1 Hubbard model in the limit $d=\infty$

A few years ago Metzner and Vollhardt [16] introduced the limit of infinite dimensionality of space $d=\infty$ for a strongly correlated electron lattice. They demonstrated that in the limit $d=\infty$ all the calculations based on the Hubbard model are greatly simplified and yet all the essential features of the model are retained. This has stimulated an enormous number of investigations that have led, in particular, to the development of rigorous mean field approximation (MFA) for different models of strongly correlated systems.

Calculations are simplified in the $d=\infty$ limit because the self-energy of an electron becomes diagonal in the site representation:

$$\Sigma_{ij}(\omega) = \Sigma(\omega)\,\delta_{ij} . \tag{3.1}$$

In other words, we can assume that the function Σ is independent of the quasimomentum and is only the function of the frequency. It is also found that in all the vertex parts of diagrams we can ignore the law of conservation of quasimomentum, i.e. we can replace the relevant δ function with unity [30].

In the limit $d=\infty$ we need to scale appropriately the parameters of the Hamiltonian. The idea of using the limit $d=\infty$ in the SCES theory goes back to the statistical mechanics in the Ising model, in which it proposed — in the case of many-dimensional space — to scale up the exchange parameter $J = J^*/z$ (here $J^* = \text{const}$ and z is the number of nearest neighbours, which tends to the limit $z \to \infty$, if $d \to \infty$). It is only this scaling that ensures a finite exchange energy density.

In the Hubbard Hamiltonian (1.1) the quantity U is a local parameter, which is independent of its environment and, therefore, it should not be scaled up. However, the matrix element of an electron jump must be scaled up in the following way [16]:

$$t = \frac{t^*}{2\sqrt{d}} , \qquad t^* = \text{const} . \tag{3.2}$$

In the case of a d-dimensional hypercubic lattice with the electron spectrum

$$\varepsilon_k = \frac{t^*}{\sqrt{d}} \sum_{\alpha=1}^{d} \cos k_\alpha , \tag{3.3}$$

the density of states $\rho_0(\omega)$ obtained in the limit $d=\infty$ is Gaussian [16]:

$$\rho_0(\omega)=\frac{1}{\sqrt{\pi}t^*}\exp\left(-\frac{\omega^2}{t^{*2}}\right) . \tag{3.4}$$

The mean-square value of the energy ε_k^2, averaged for this density, is t^{*2}, i.e. it is finite in the limit $d\to\infty$, which justifies the selection of scaling described by formula (3.2). It also agrees with the circumstance that if $U\gg t$, the effective exchange integral for the nearest neighbours obeys $J\sim t^2/U\sim 1/z$, as expected for the exchange Hamiltonian.

Therefore, in the limit $d=\infty$, all the Van Hove singularities of the density of states disappear, which distinguishes this limit from the finite number of dimensions $d=2$ or 3. Another difference is that the spectrum described by expression (3.4) is not bounded, in contrast to the band spectrum for a lattice of finite dimensions. These two circumstances are unimportant from the theoretical point of view. The most important characteristic of the limit $d=\infty$ is the local nature of the self-energy.

It follows from the scaling of the hopping parameter, described by formula (3.2) that the dependence, on d, of the single-particle Green function for a lattice $G_{ij}^0(z)$ is governed, in the limit $d=\infty$, by the 'distance' between the sites i and j:

$$G_{ij}^0\sim\left(\frac{1}{\sqrt{d}}\right)^{|i-j|} , \quad |i-j|=\sum_{\alpha=1}^{d}|i_\alpha-j_\alpha| , \tag{3.5}$$

where the coordinates of the sites are expressed in terms of the lattice parameter. In particular, for the nearest neighbours we have $G_{ij}^0\sim d^{-1/2}$.

In accordance with the general concept of statistical mechanics, the limit $d=\infty$ corresponds to the mean field theory, which is not trivial in the Hubbard model. We shall now consider several versions of this theory. Its formulation is closely related to the coherent potential approximation, which we shall now consider. This makes it possible to relate the Hubbard-3 approximation to the limit $d=\infty$.

3.2 Coherent potential approximation for disordered systems

In some approaches employed in the SCES theory (decoupling of the Green functions and functional integration), successful use has been made of the 'alloy analogy' between the motion of an electron over the lattice sites, which are occupied by electrons with one or the other spin orientation, and the motion of an electron in a disordered binary alloy. In the latter case the Green function of an electron can be calculated in the coherent potential approximation (CPA).

The central feature of this method is the assumption that the self-energy of an electron can be regarded as diagonal in the site representation [32, 35], i.e.

$$\Sigma_{ij}=\Sigma\delta_{ij} . \tag{3.6}$$

This relationship applies specifically in the limit $d=\infty$. It therefore becomes clear that the CPA is exact in the infinite-dimensional limit. Recognition of this fact has made it possible to develop the mean field approximation for the Hubbard model, which is exact in the limit $d=\infty$.

We can understand better the meaning of the limit $d=\infty$ in the theory of interacting electrons if we consider first the corresponding limit for a system of noninteracting electrons moving on a lattice with a random atomic potential:

$$H=t\sum_{i,j}C_i^\dagger C_j+\sum_i V_i n_i \tag{3.7}$$

(the spin indices are omitted, because V_i is independent of spin).

We shall denote the configurational averaging of random quantities by $\langle\ldots\rangle_{\rm av}$. The task is to calculate the quantity $\langle G\rangle_{\rm av}$, where G is the one-electron Green function corresponding to the Hamiltonian (1.1). In the site represent-ation the Green function G obeys the equation

$$G=G^0+G^0VG . \tag{3.8}$$

We shall introduce the self-energy Σ of an electron in an effective medium described by the average Green function, using the relationship

$$\langle G\rangle_{\rm av}=(G_0^{-1}-\Sigma)^{-1} . \tag{3.9}$$

We now have to find self-consistently the energy Σ.

If we combine expressions (3.8) and (3.9), we can represent G in the form

$$G=\langle G\rangle_{\rm av}+\langle G\rangle_{\rm av}T\langle G\rangle_{\rm av} , \tag{3.10}$$

where

$$T=\frac{V-\Sigma}{1-(V-\Sigma)\langle G\rangle_{\rm av}} \tag{3.11}$$

is the T matrix. Expression (3.10) is not self-contradictory if we assume that $\langle T\rangle_{\rm av}=0$.

In the limit $d=\infty$, the self-energy part Σ_{ij} is diagonal in the site representation and it is independent of k in the momentum representation. Therefore, it follows from relationship (3.9) that

$$\big\langle G(\omega)\big\rangle_{\rm av}=G_{ii}^0(\omega-\Sigma) , \tag{3.12}$$

where

$$G_{ii}^0=\frac{1}{N}\sum_{\boldsymbol{k}}\frac{1}{\omega-\varepsilon_{\boldsymbol{k}}}=\int \mathrm{d}\varepsilon\,\frac{\rho_0(\varepsilon)}{\varepsilon-\omega} \tag{3.13}$$

is the single-site Green function of an ideal lattice and $\rho_0(\varepsilon)$ is the density of electron states in this lattice.

We shall now write down the final equation for the effective self-energy part:

$$\left\langle\frac{V_i-\Sigma(\omega)}{1-\big(V_i-\Sigma(\omega)\big)G_{ii}^0\big(\omega-\Sigma(\omega)\big)}\right\rangle_{\rm av}=0 . \tag{3.14}$$

This is the main equation in the CPA approach. It is exact in the limit $d=\infty$.

The free energy F can be written as a sum of three contributions: the free energy $F_{\rm med}$ of an effective homogeneous medium, from which it is necessary to subtract the self-energy F_i at a site i, and to replace it with the energy characterised by the total potential V_i at a site i, which is averaged over the configurations. The sum is thus

$$F=F_{\rm med}-F_i+\langle F_i'\rangle_{\rm av} , \tag{3.15}$$

where

$$F_{\rm med}=-T\sum_{\boldsymbol{k}}\left[G^0(\boldsymbol{k},\mathrm{i}\omega_k)-\Sigma\right]^{-1} , \tag{3.16}$$

$$F_i = -T \operatorname{Tr} \ln \langle G_{ii} \rangle_{\mathrm{av}}^{-1} , \tag{3.17}$$

$$F_i' = -T \operatorname{Tr} \ln \left[\langle G_{ii} \rangle_{\mathrm{av}}^{-1} - V_i - \Sigma \right] . \tag{3.18}$$

Introduction of a local effective propagator,

$$\mathcal{G}^{-1} \equiv \langle G_{ii} \rangle_{\mathrm{av}}^{-1} + \Sigma , \tag{3.19}$$

makes it possible to represent the free energy in the form

$$F = -T \operatorname{Tr} \left\{ \int \mathrm{d}\varepsilon \, \rho_0(\varepsilon) \ln(\mathrm{i}\omega_k + \mu - \Sigma - \varepsilon) \right.$$
$$\left. - \ln(\mathcal{G}^{-1} - \Sigma) + \left\langle \ln(\mathcal{G}^{-1} - V_i) \right\rangle_{\mathrm{av}} \right\} . \tag{3.20}$$

Minimisation of the functional (3.20) by means of the condition $\delta F / \delta \mathcal{G}^{-1} = 0$ yields the equation

$$\frac{1}{\mathcal{G} - \Sigma} = \left\langle \frac{1}{\mathcal{G} - V_i} \right\rangle_{\mathrm{av}} , \tag{3.21}$$

which together with Eqn (3.19) determines the value of Σ. Eqn (3.21) is identical with the equation (3.14) identified earlier. Eqns (3.19) and (3.21) have to be solved by iteration. Eqn (3.21) is used to find Σ for a given value of $\mathcal{G}$. Then Eqn (3.19) is applied to obtain a new value of $\mathcal{G}^{-1}$. This value is then substituted in Eqn (3.21) and so on, until self-consistent solutions are obtained. Eqns (3.19) and (3.21) are equations of the mean field theory for the Hamiltonian (3.7). They are exact in the limit $d = \infty$.

The corresponding equations for the Hubbard model can be obtained by the same scheme. Complete analogy between the model represented by Eqn (3.7) and the Hubbard model requires a somewhat different (and fairly formal) representation of the contribution F_i' to the free energy [33]:

$$F_i' = -T \ln Z_i' . \tag{3.22}$$

Here, Z_i' is the partition function, defined with the aid of the action S_i':

$$Z_i' = \int \mathrm{D}\psi \, \mathrm{D}\psi^* \exp\left[S_i'(\psi, \psi^*) \right] , \tag{3.23}$$

$$S_i' = \operatorname{Tr} \psi_n^* \langle G_{ii} \rangle_{\mathrm{av}}^{-1} \psi_n - \operatorname{Tr} \psi_n^* (V_i - \Sigma) \psi_n , \tag{3.24}$$

where ψ and ψ^* are the Grassmann variables.

Expression (3.24) has the form of a Lagrangian. Since this expression is bilinear in ψ and ψ^*, the functional integral (3.23) is readily calculated and the result is expression (3.18) for F_i'. A simple generalisation of expressions (3.23) and (3.24) gives the free energy for the model of interacting electrons.

3.3 Reduction of the Hubbard model in the limit $d = \infty$ to the one-impurity Anderson model

The single-site action for the Hamiltonian (1.1) should be written in the form [33]

$$S_i' \{ \psi_\sigma, \psi_\sigma^*; \mathcal{G}_\sigma^{-1} \} = \operatorname{Tr} \psi_{\sigma n}^* \mathcal{G}_\sigma^{-1} \psi_{\sigma n}$$
$$- U \int_0^\beta \mathrm{d}\tau \, \psi_\uparrow^*(\tau) \psi_\uparrow(\tau) \psi_\downarrow^*(\tau) \psi_\downarrow(\tau) , \tag{3.25}$$

where $\beta = 1/kT$ and k is the Boltzmann constant.

The partition function Z_i' can be calculated with the aid of the Hubbard–Stratonovich formula

$$\exp a^2 = \int_{-\infty}^{\infty} \mathrm{d}x \, \exp(-\pi x^2 - 2\sqrt{\pi} a x) , \tag{3.26}$$

which transforms an exponential function with a quadratic operator to an exponential function with a linear operator.

The identity

$$n_{i\uparrow} n_{i\downarrow} = \frac{1}{4} \left[(n_{i\uparrow} + n_{i\downarrow})^2 - (n_{i\uparrow} - n_{i\downarrow})^2 \right]$$

can be used to transform the exponential function in the expression for Z_i' into a functional integral in terms of classical fields $\xi(\tau)$ and $\eta(\tau)$, which describe fluctuations of the charge and spin densities, respectively:

$$\exp\left[-U \int_0^\beta \mathrm{d}\tau \, n_{i\uparrow}(\tau) \, n_{i\downarrow}(\tau) \right]$$
$$= \int \delta\eta \, \delta\xi \exp\left\{ -\frac{1}{2\beta} \int_0^\beta \mathrm{d}\tau \left[\eta^2(\tau) + \xi^2(\tau) \right] - \sqrt{\frac{2U}{\beta}} \right.$$
$$\left. \times \left[\mathrm{i}\xi(\tau) \left(n_\uparrow(\tau) + n_\downarrow(\tau) \right) + \eta(\tau) \left(n_\uparrow(\tau) - n_\downarrow(\tau) \right) \right] \right\} . \tag{3.27}$$

Expansion of the fields $\xi(\tau)$ and $\eta(\tau)$ as a Fourier series in terms of discrete frequencies ω_k gives the final expression for Z_i' as a functional integral in terms of the fields ξ_n and η_n:

$$Z_i' = \int \delta\eta \, \delta\xi \exp\left[S_i'(\eta, \xi; \mathcal{G}_\sigma^{-1}) \right] , \tag{3.28}$$

$$S_i' = -\frac{1}{2} \sum_{n=-\infty}^{\infty} (\xi_n^2 + \eta_n^2) + \operatorname{Tr} \ln \left[\hat{\mathcal{G}}_\sigma^{-1} - \sqrt{\frac{U}{2\beta}} (\sigma \hat{\eta} + \mathrm{i}\hat{\xi}) \right] . \tag{3.29}$$

Here $\hat{\xi}$ and $\hat{\eta}$ are infinite-series matrices with the elements $\hat{\xi}_{mn} = \xi_{m-n}$, $\hat{\eta}_{mn} = \eta_{m-n}$, and $\hat{\mathcal{G}}_\sigma^{-1}$ is the following diagonal matrix:

$$(\hat{\mathcal{G}}_\sigma^{-1})_{mn} = \delta_{mn} \mathcal{G}_\sigma^{-1}(\mathrm{i}\omega_n) .$$

The total free energy has three contributions, as in Ref. [59]:

$$F = -T \operatorname{Tr} \left\{ \int \mathrm{d}\varepsilon \, \rho_0(\varepsilon) \, \ln(\mathrm{i}\omega_n + \mu - \Sigma_\sigma - \varepsilon) \right.$$
$$\left. - \ln(\mathcal{G}_\sigma^{-1} - \Sigma_\sigma) \right\} - T \ln Z_i' , \tag{3.30}$$

where the effective local propagator is

$$\mathcal{G}_\sigma^{-1} = \frac{1}{G_{ii,\sigma}^0} \left[\omega - \Sigma_\sigma(\omega) \right] + \Sigma_\sigma(\omega) . \tag{3.31}$$

Differentiation of Eqn (3.31) with respect to $\mathcal{G}_\sigma^{-1}$ gives the following equation for the self-energy part Σ_σ:

$$\frac{1}{\mathcal{G}_\sigma^{-1}(\mathrm{i}\omega_n) - \Sigma_\sigma(\mathrm{i}\omega_n)} = \left\langle \left[\frac{1}{\mathcal{G}_\sigma^{-1} - \sqrt{U/2\beta}(\sigma\hat{\eta} + \mathrm{i}\hat{\xi})} \right]_{nn} \right\rangle_{\eta\xi} . \tag{3.32}$$

Here, the symbol $\langle \ldots \rangle$ represents averaging (functional integration) over the variables η and ξ:

$$\langle \ldots \rangle_{\eta\xi} = \frac{1}{Z_i'} \int \delta\eta \, \delta\xi \ldots \exp\left(S_i'[\eta, \xi] \right) .$$

Eqns (3.31) and (3.32) are self-consistent equations for determination of the quantities Σ_σ and $\mathcal{G}_\sigma^{-1}$. They can be solved by iteration. A given value of $\mathcal{G}_\sigma^{-1}$ is used in Eqn (3.32) to find Σ_σ. Then, the new value of Σ is used in Eqn (3.31) to calculate $\mathcal{G}_\sigma^{-1}$, and the process is repeated.

Eqns (3.31) and (3.32) have similar structures to Eqns (3.19) and (3.21) used in the model described by Eqn (3.7). In both models, averaging over Σ is carried out on the right-hand sides of the equations: in one case the averaging is over configurations of the local fields V_i with a certain given distribution function, and in the other case the averaging is over an infinite set of fluctuation fields η_ν and ξ_ν, which are characterised by discrete frequencies ω_ν.

There is however an important difference between the two models: for a system of noninteracting electrons in a disordered medium all the functions $\mathcal{G}^{-1}(\omega)$ and $\Sigma(\omega)$ have the same frequency. In Eqn (3.32) for a system of interacting electrons the frequencies are intermingled. Therefore, the dynamics of the Hubbard model in the limit $d=\infty$ is nontrivial even in the static case when $\eta_\nu = \xi_\nu = 0$ for $\nu \neq 0$.

Eqns (3.31) and (3.32) represent the truly thermodynamically self-consistent mean field theory for the Hubbard model. It is exact in the zeroth approximation in terms of the parameter $1/z$. The theory is valid for an arbitrary parameter U and an arbitrary electron density n. It differs funda-mentally from other self-consistent approaches, for example those of the Hartree–Fock type which are always of limited validity in the space of the parameters of the system.

Two quantities in this theory, Σ_σ and $\mathcal{G}_\sigma$, represent a homogeneous effective medium. The mean field exerted on an electron by other electrons is represented by Σ_σ, whereas $\mathcal{G}_\sigma$ determines the exact local propagator:

$$G_{ii,\sigma} = \left(\mathcal{G}_\sigma^{-1} - \Sigma_\sigma\right)^{-1} . \tag{3.33}$$

We can see that in the limit $d=\infty$ we face the problem of the interaction of electrons at one site immersed in a system of effectively noninteracting electrons. The solution of this problem requires calculation of the third-order contribution to the free energy described by expression (3.30). Its calculation, i.e. effective averaging of the right-hand side of Eqn (3.32), presents the greatest difficulty in this theory. It is because of this contribution that the Hubbard model cannot be solved analytically in the limit $d=\infty$.

Only the exact equations (3.31) and (3.32) are obtained in the limit $d=\infty$ and the problem is thus reduced to that of numerical calculations. However, in practice it is more convenient to proceed differently. It is possible to reduce the problem of a lattice with local interactions (Hubbard model) to the problem of a single impurity immersed in a specially selected system of noninteracting electrons in the same lattice. This approach had been suggested simultaneously in Refs [34–36].

Let us go back to Eqn (3.25) for the single-site action. The quantity $\mathcal{G}_0$ is not yet determined. In the treatment discussed earlier it has been found by minimisation of the free energy. However, here we shall proceed differently. We shall consider Eqn (3.25) as representing the action in the case of a single-impurity problem in a certain model (Anderson model [4] or Wolff model [37]). This action can be used to calculate the electron Green function for an auxiliary single-impurity problem $G_{\text{imp}}(\mathrm{i}\omega_n, \mathcal{G}^{-1})$ and its self-energy part $\Sigma_{\text{imp}}(\mathrm{i}\omega_n, \mathcal{G}^{-1})$ with a given bare Green function $\mathcal{G}$.

If we identify G_{imp} and $\Sigma_{\text{imp},\sigma}$ with, respectively, the local Green function G_{ii} and the self-energy Σ in the Hubbard model, we can write down an equation for self-consistent determination of the quantity $\mathcal{G}$:

$$\frac{1}{\mathcal{G}^{-1} - \Sigma} = \int \mathrm{d}\varepsilon \, \frac{\rho_0(\varepsilon)}{\mathrm{i}\omega_n + \mu - \Sigma - \varepsilon} . \tag{3.34}$$

The new refined value of $\mathcal{G}$ can be used to solve again the auxiliary single-impurity problem, i.e. it can be used to find G and Σ, and then Eqn (3.4) gives the new value of $\mathcal{G}$. This iteration procedure has to be repeated until a stable (self-consistent) result is obtained.

It is possible to adopt also a different approach which can be used to study the qualitative nature of the solution of the equations in the Hubbard model when $d=\infty$. This can be done with the aid of the bare Green function in single-impurity models. In the Anderson model, we have

$$\mathcal{G}^{-1}(\omega) = \omega - \varepsilon_d + V^2 \int \mathrm{d}\varepsilon \, \frac{\Delta(\varepsilon)}{\omega - \varepsilon} , \tag{3.35}$$

where

$$V^2 \Delta(\varepsilon) = \pi \sum_k V_k^2 \, \delta(\varepsilon - \varepsilon_k) ,$$

ε_d is the energy of a level d of an impurity atom, and V_k is the $s-d$ hybridisation parameter. In the Wolff model, we find that

$$\mathcal{G}^{-1}(\omega) = \int \mathrm{d}\varepsilon \, \frac{\Delta(\varepsilon)}{\omega - \varepsilon} . \tag{3.36}$$

It follows that in the limit $d=\infty$ the Hubbard model reduces to one of the models for an impurity atom in a lattice. The bare Green function $\mathcal{G}_\sigma$ for the single-impurity problem takes account of all the effective interactions of an electron at an impurity site with the rest of the crystal lattice.

The single-impurity Anderson model cannot be solved exactly, but one can use the results of its renormalisation-group analysis [38]. Depending on the ratio of the main parameters E_d and Δ (E_d is the renormalised energy of the d level and Δ is the width of this level), three types of Fermi-liquid behaviour may be expected in the Anderson model. They correspond to three types of Fermi-liquid behaviour in the Hubbard model, described below.

(1) If $E_d/\Delta \ll -1$, then near the half-filled configuration the density of states $\rho(\omega)$ obtained in the Anderson model has a three-peak structure: a narrow quasistatic peak (Suhl–Abrikosov resonance) of width T_k (Kondo temperature) and two satellite peaks. In the Hubbard model they correspond to the second Hubbard subband for particles (upper satellite) and holes (lower satellite). This is the case of localised magnetic moments. The spin dynamics involves fluctuations between the states $|\uparrow\rangle$ and $|\downarrow\rangle$ at a site.

(2) If $|E_d/\Delta| < 1$, we are dealing with the mixed-valence case, when transitions between the following three states are important: $|0\rangle$, $|\uparrow\rangle$ and $|\downarrow\rangle$. The density of states $\rho(\omega)$ has two peaks: a broadened quasiparticle peak and a satellite; in the Hubbard model this corresponds to two fairly wide Hubbard subbands.

(3) Finally, when $E_d/\Delta \gg 1$, the density of states $\rho(\omega)$ has one broadened peak. It should correspond to an unsplit subband in the Hubbard model.

3.4 Properties of the Hubbard model in the limit $d = \infty$

Numerical calculations based on the algorithm described by Eqn (3.4), which includes calculations based on an auxiliary single-impurity problem, confirm the above-described qualitative pattern of the structure of the spectrum in the Hubbard model considered in the mean field approximation [24–41, 43, 44]. Figs 4 and 5 illustrate the three types of the Fermi liquid behaviour, which appears in the Hubbard model for a half-filled band when U is increased.

The results presented in Fig. 4 represent the solution of the single-impurity Anderson model problem by the quantum Monte Carlo method, which is exact but cannot be used at low temperatures [34]. The results in Fig. 5 were obtained for $T = 0$ by combination of the quantum Monte Carlo method and several series found by perturbation theory in terms of the parameter U [42]. In contrast to Ref. [34], the solution given in Ref. [42] has a gap corresponding to the metal–insulator transition and it also predicts an intermediate case between the metal and insulator states.

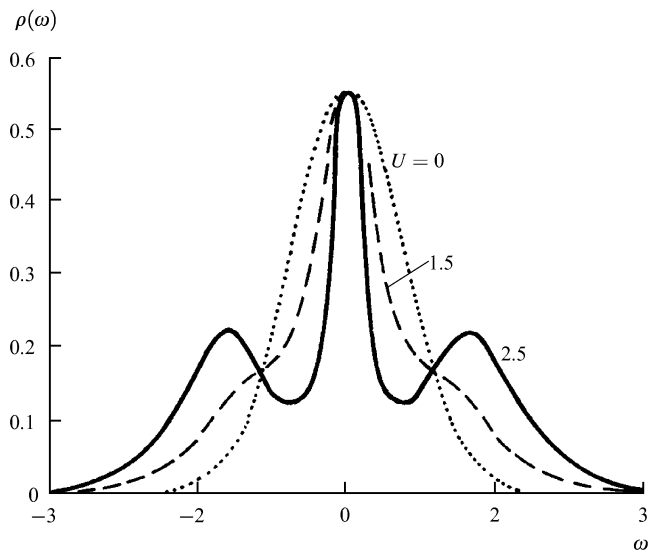

Figure 4. Spectral density of the local Green function $G_{ii}(\omega)$ in the Hubbard model, obtained in the mean field approximation for various values of U when $n = 1$ [34].

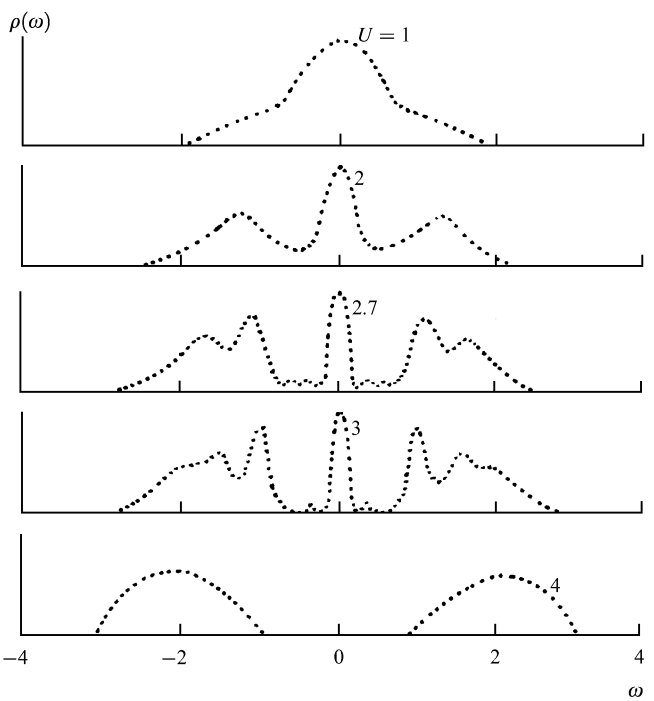

Figure 5. Same as in Fig. 4 [42].

The amplitude of the narrow central peak varies as U rises to its critical value U_c, when a gap appears in the spectrum and the central peak disappears abruptly. Therefore, if $d = \infty$ and $T = 0$, the Hubbard model predicts a gradual metal–insulator transition. The numerical results of Refs [34, 42] had been supplemented by a simple analytic calculation [41], which helps to understand the physics of the phenomena. The three peak structure of the local density of states can be approximated by a bare Green function of the type

$$\mathcal{G}(\omega) = \left(\omega - \frac{W\Delta}{\omega + \mathrm{i}\Delta\,\mathrm{sgn}\,\omega}\right)^{-1} . \tag{3.37}$$

Then, as $\Delta \to 0$, we find that $\Delta \to 0\,\mathrm{Im}\,\mathcal{G}(\omega)$ does indeed describe a δ-like peak of width Δ at the point $\omega = 0$ and two satellite peaks at points $\omega = \pm\omega_0$, where $\omega_0^2 = W\Delta - \Delta^2/2$. In this way the bare Green function $\mathcal{G}$ is renormalised by the quantity Δ, which should be found from the self-consistency equation (3.34) by an iteration process.

If the self-energy $\Sigma_{\mathrm{imp}}(\omega)$ is calculated first, the iteration process can be represented by

$$\Delta_{n+1} = \frac{9W}{U^2}\left(W\Delta_n - \frac{\Delta_n^2}{2}\right) .$$

The above system of nonlinear equations has two fixed points:

$$\Delta^* = \begin{cases} 2W\left[1 - \left(\dfrac{U}{U_c}\right)^2\right], & U < U_c , \\ 0 , & U > U_c . \end{cases} \tag{3.38}$$

The regions of stability are separated by the critical value $U_c = 3W$. The zero fixed point corresponds to an insulator and the nonzero point represents a metal. Since it follows from the definition of the Green function (3.37) that for $\omega < \Delta$, we have

$$\mathrm{Re}\,\Sigma(\omega) \approx \frac{W}{\Delta}\,\omega ,$$

it follows that for the metal phase the Migdal parameter in the vicinity of the phase transition is

$$Z \approx 1 - \left(\frac{U}{U_c}\right)^2 . \tag{3.39}$$

It follows that as the phase transition is approached from the low-U side, the system remains a Fermi liquid and it gradually transforms into an insulator. These heuristic results are confirmed by numerical solutions of the exact equations in the Hubbard model for $d = \infty$ [42] (Fig. 6).

In the limit $d = \infty$ the magnetic properties of the Hubbard model for the half-filled case exhibit characteristics of a localised antiferromagnet, which is to be expected. A numerical calculation of the static magnetic susceptibility for the wave vector $q = Q$ at different temperatures reveals a divergence when a certain point T_N is

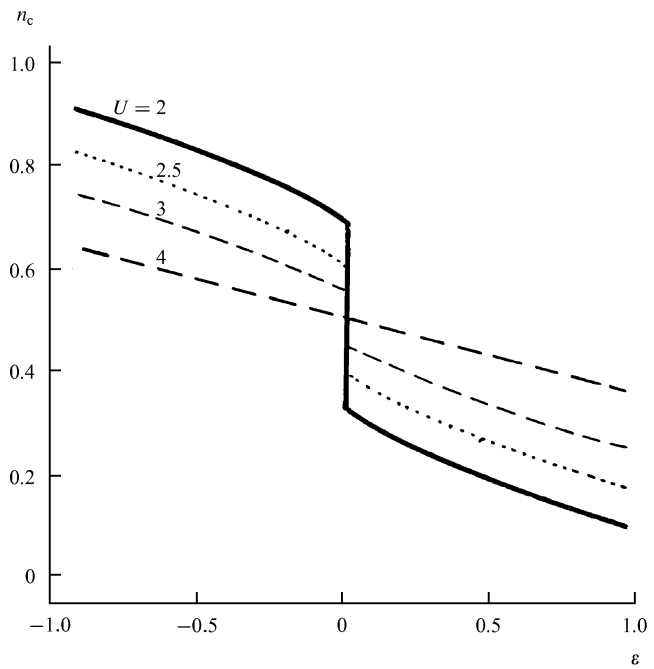

Figure 6. Band filling n_c as a function of ε near the Fermi energy, calculated for various values of U when $n = 1$ [42].

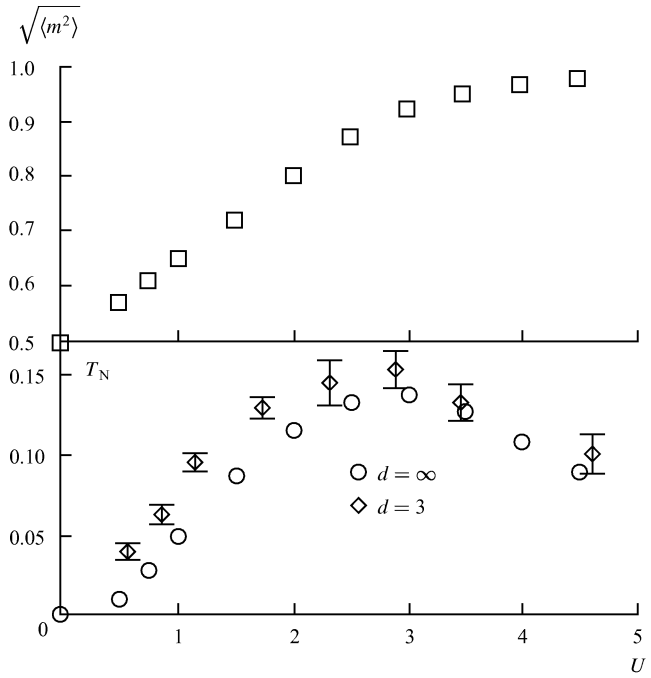

Figure 7. Local magnetic moment and the Neel temperature, plotted as a function of the parameter U for $n = 1$ [44].

approached [35, 44]. For $U = 1.5$, the static magnetic susceptibility is

$$\chi(\boldsymbol{Q}) \propto (T - T_N)^{-\nu} , \tag{3.40}$$

where $T_N = 0.0866 \pm 0.0003$, and $\nu = 0.99 \pm 0.05$. Therefore, the Curie law is satisfied here, as in the case of the isotropic Heisenberg model with an infinite number of nearest neighbours.

The behaviour of the Neel temperature T_N is plotted as a function of the parameter U in Fig. 7. At low values of U the Neel temperature T_N is exponentially small, which agrees with the perturbation theory results [45]. At very high values of U the Neel temperature obeys $T_N \propto 1/U$, which is in agreement with the well-known results [45]. Fig. 7 includes also the results of a numerical calculation of the case when $d = 3$, which show that the limit of infinite dimensions of space $d = \infty$ is very close to the real dimensions.

Fig. 7 gives also the dependence on U of the rms localised moment

$$\left(\langle m^2 \rangle\right)^{1/2} = \left(\langle (n_\uparrow - n_\downarrow)^2 \rangle\right)^{1/2} = \left(1 - 2\langle n_\uparrow n_\downarrow \rangle\right)^{1/2} . \tag{3.41}$$

When the parameter U is varied from 0 to infinity, the localised moment $\left(\langle m^2 \rangle\right)^{1/2}$ varies from 0.5 to 1. The behaviour of $\left(\langle m^2 \rangle\right)^{1/2}$ is correlated with the dependence of T_N on U: the Neel temperature passes through a maximum exactly where the localised moment begins to saturate.

The Neel temperature T_N begins to fall steeply away from the half-filled case. The critical values of the parameter U corresponding to the appearance of a divergence in the antiferromagnetic susceptibility are plotted in Fig. 8. However, in the case of the ferromagnetic susceptibility no divergence has been found for any of the parameters used in the calculations.

The change in the spectral or density of states $\rho(\omega)$ as a result of deviation from the half-band filling is plotted in Fig. 9 for $U = 4$, which corresponds to the insulator state

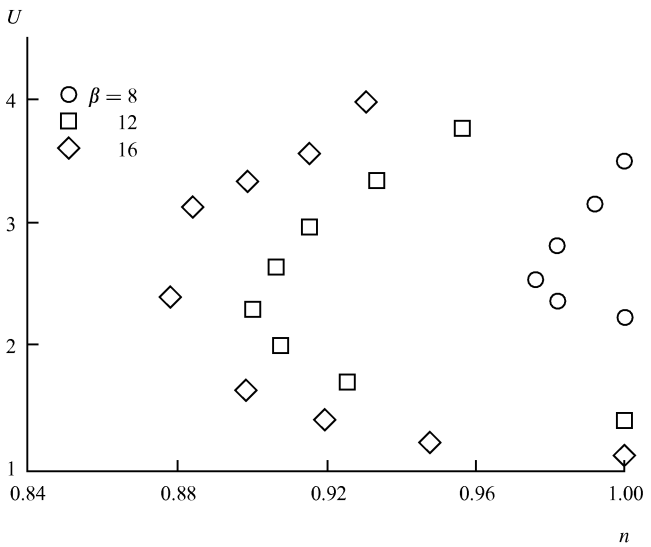

Figure 8. Critical values of U at which a divergence appears in the magnetic susceptibility, plotted as a function of the electron density n ($\beta = 16$) in units of the band width [44].

when $n = 1$. The insulator gap in the spectrum disappears away from $n = 1$ and it is replaced by a central peak of amplitude which increases at the expense of the amplitudes of the satellites. The same peak arises as a result of cooling (Fig. 10). In this range of temperatures the amplitude of the peak is a function of $\ln T$.

On the other hand, the large satellite peaks corresponding to transitions accompanied by a reduction in the charge (transitions to a site and from a site) change little with temperature. The quasiparticle peak associated with the scattering of an electron on the Fermi surface by spin fluctuations increases considerably in amplitude as a result of cooling, exactly as in the Kondo effect. A Kondo-like

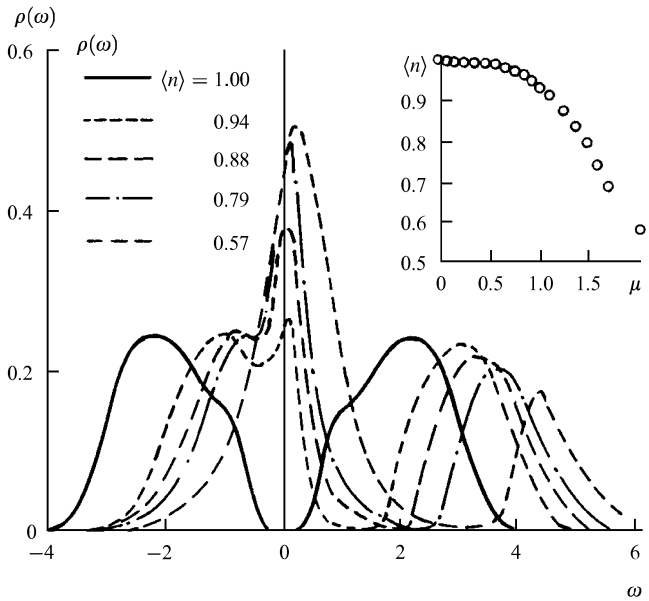

Figure 9. Evolution of the density of states as a result of deviation from the half-filled band case, plotted for $\beta = 7.2$ and $U = 4$. The inset is the dependence of the chemical potential on the electron density.

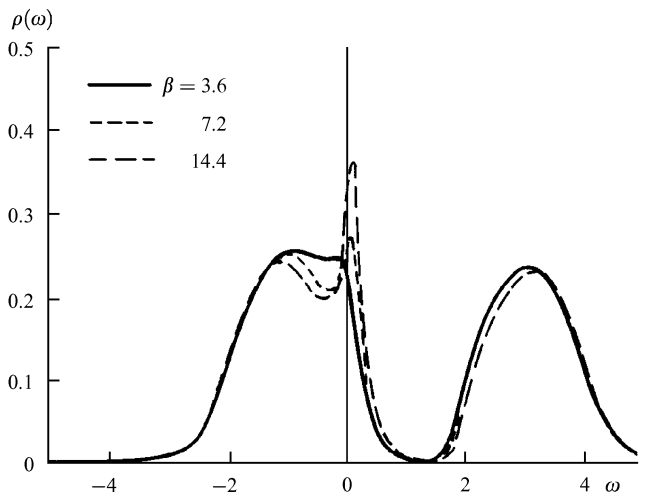

Figure 10. Evolution of a resonance peak on the Fermi surface plotted as a function of temperature for $U = 4$ and $n = 0.94$ [44].

resonance on the Fermi surface of such a system should give rise to significant anomalies of thermodynamic and transport properties, such as the specific heat, electric resistance, optical conductivity, etc. [43].

In this section we have thus demonstrated that in the limit of infinite dimensionality of space the Hubbard model is equivalent to the single-impurity Anderson model with specially selected characteristics. The behaviour of the Hubbard model is governed by the physical properties of the single-impurity Anderson model, which have been investigated quite thoroughly.

We have found that in the limit $d = \infty$ the Hubbard model predicts the metal–insulator phase transition near the half-filling of the relevant band. If U is sufficiently large, antiferromagnetic ordering with localised magnetic moments appears in the insulator phase. The metal phase

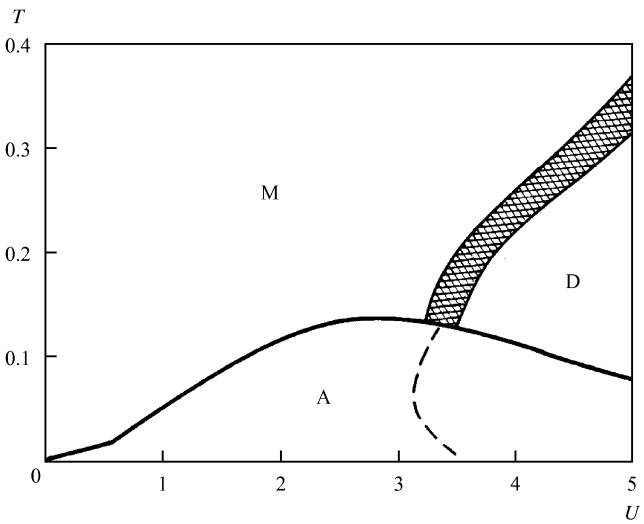

Figure 11. Phase diagram in the (T, U) plane, obtained in the Hubbard model for $d = \infty$, $n = 1$ [43].

exhibits Fermi-liquid behaviour of heavy electrons, the mass of which increases on approach to the boundary of the insulator phase.

The expected phase diagram for the half-filled case is presented in Fig. 11 where the roughly estimated region of the transition from the metal (M) to the insulator (I) phase is shown shaded. This region represents evidently a semimetallic state with thermodynamically excited carriers.

Deviation from the high-filled case results in rapid replacement of the insulator by the metal phase with enhanced Fermi-liquid parameters. In particular, low-temperature narrow resonances appear on the Fermi surface and they correspond to the Kondo screening of localised magnetic moments. The antiferromagnetic ordering is suppressed on deviation from $n = 1$. If $n \leqslant 0.8$, such a system behaves as an ordinary Fermi liquid.

It should be stressed that in the limit $d = \infty$ we can derive the exact equation for the Hubbard model, although in the derivation of the solution it is necessary to solve numerically the auxiliary problem of the single-impurity Anderson model. If this is done, then the result is the exact mean field theory for the Hubbard model. It follows that, at least in principle, we know the exact solutions of the model in two limiting cases: $d = 1$ [46, 47] and $d = \infty$.

This gives rise to a natural question: how close is the behaviour of the model for $d = 3$ to the case when $d = \infty$? There is as yet no complete answer to this question, but the experience accumulated in studies of strongly correlated systems in the limit $d = \infty$ allows us to conclude that even the three dimensions of real space $(d = 3)$ can be regarded as a very high number of such dimensions. Some comparisons of the results of calculations for $d = \infty$ and $d = 3$ confirm this (see, for example, Fig. 7).

3.5 Breakdown of the Fermi-liquid behaviour of the model

The quantum Monte Carlo method has been used above in presentation of the exact, in the limit $d = \infty$, theory needed in the solution of the effective single-impurity problem. Since in numerical calculations one deals with discrete Matsubara frequencies $\omega_n = 2\pi nT$, this quantum method has a limit on the low-temperature side. The need to carry

out numerical calculations of continuation from the imaginary to the real axis increases the calculation difficulties. Therefore, it is necessary to look for new approximate calculation schemes.

The Edwards–Hertz approximation (EHA) [48] has proved very effective. These authors developed an interpolation scheme exact in the two limits: in the atomic limit ($t \to 0$) and in the limit of free electrons ($U \to 0$). Edwards and Hertz used this approximation to reveal breakdown of the Fermi-liquid behaviour of the electron states at intermediate values of U.

Recently, Wermbter and Czycholl [49] put forward an improved version of the EHA method and carried out detailed calculations of $\rho(\omega)$, $\operatorname{Im}\Sigma(\omega)$, $\operatorname{Re}\Sigma(\omega)$ for a wide range of the parameters U, n and T. As a result of their investigation the physical picture of the transition of such a system, due to variation of U or n, from the Fermi-liquid behaviour to the insulator phase across a region of non-Fermi-liquid states has become much clearer. We shall now give the main results of Refs [48, 49].

We shall consider again the limit $d = \infty$. The single-site Green function of the system $G_{ii\sigma}(\omega)$, which for brevity will be denoted by $G_\sigma(\omega)$, can be expressed in terms of the density of states $\rho_0(\omega)$ of noninteracting electrons by means of the relationship

$$G_\sigma(\omega) = \int_{-\infty}^{\infty} \mathrm{d}\varepsilon \, \frac{\rho_0(\varepsilon)}{\omega - \Sigma_\sigma(\omega) - \varepsilon} \, . \tag{3.42}$$

Following Ref. [49], we shall represent the self-energy part in the form

$$\Sigma_\sigma(\omega) = \frac{U n_{-\sigma}}{1 - \left[U - \Sigma_\sigma(\omega)\right] \tilde{G}_\sigma(\omega)} \, , \tag{3.43}$$

$$n_\sigma = \int_{-\infty}^{\infty} \mathrm{d}\varepsilon \, \rho_{0\sigma}(\varepsilon) \, f(\varepsilon) \, . \tag{3.44}$$

Here, $\rho_\sigma(\omega) = -(1/\pi) \operatorname{Im} G_\sigma(\omega)$ is the density of states deduced taking into account the interaction of electrons and the quantity $\tilde{G}_\sigma(\omega)$ should be defined additionally. We note that if $\tilde{G}_\sigma(\omega)$ is replaced with $G_\sigma(\omega)$, expression (3.43) reduces to the equation obtained in the CPA approximation, corresponding to the 'alloy analogy' in the Hubbard model (Hubbard-3 approximation).

Following the ideas of Edwards and Hertz [48], it is necessary to select $\tilde{G}_\sigma(\omega)$ so that expression (3.43) reduces in the atomic limit to the expression obtained by the CPA method and in the limit $U \to 0$ it becomes the well-known expression for the self-energy obtained from standard perturbation theory.

It is easily shown that both limits are satisfied if $\tilde{G}_\sigma(\omega)$ is selected in the form

$$\tilde{G}_\sigma(\omega) = \int_{-\infty}^{\infty} \mathrm{d}\varepsilon \, \frac{\tilde{\rho}_0(\varepsilon)}{\omega - \Sigma_\sigma(\omega) + E_\sigma - \varepsilon} \, , \tag{3.45}$$

$$\begin{aligned} \tilde{\rho}_0(\omega) = {} & \frac{1}{n_{-\sigma}(1 - n_{-\sigma})} \int \mathrm{d}\omega_1 \, \mathrm{d}\omega_2 \, \mathrm{d}\omega_3 \\ & \times \rho^0_{-\sigma}(\omega_1 - E_{-\sigma}) \, \rho^0_{-\sigma}(\omega_2 - E_{-\sigma}) \, \rho^0_\sigma(\omega_3 - E_\sigma) \\ & \times \left\{ f(\omega_1)\left[1 - f(\omega_2)\right] + f(\omega_3)\left[f(\omega_2) - f(\omega_1)\right] \right\} \\ & \times \delta(\omega + \omega_1 - \omega_2 - \omega_3) \, . \end{aligned} \tag{3.46}$$

Here, the shift E_σ, leading to an effective atomic level for the σ electrons, can be calculated in a self-consistent manner from the condition

$$n_\sigma = \int_{-\infty}^{\infty} \mathrm{d}\omega \, \rho_\sigma(\omega) \, f(\omega) = \int_{-\infty}^{\infty} \mathrm{d}\omega \, \rho^0_\sigma(\omega - E_\sigma) \, f(\omega) \, . \tag{3.47}$$

Since in the atomic limit the density of states $\rho_\sigma(\omega)$ becomes the δ function, formula (3.46) reduces to $\tilde{\rho}_\sigma(\omega) = \rho_0(\omega - E_\sigma)$ and we then obtain from expression (3.45) the following:

$$\tilde{G}_\sigma(\omega) = G^0\left[\omega - \Sigma_\sigma(\omega)\right] = G_\sigma(\omega) \, ,$$

which gives the CPA result (Hubbard-3 approximation).

On the other hand, if expression (3.43) is expanded in powers of the parameter U, the result is

$$\Sigma_\sigma(\omega) = U n_{-\sigma} + U^2 n_{-\sigma}(1 - n_{-\sigma}) \, \tilde{G}_\sigma(\omega) \, , \tag{3.48}$$

which — subject to the definitions (3.45) and (3.46) — reduces to the perturbation theory result. Eqns (3.42)–(3.47) should be solved by interpolation with the aid of a Gaussian bare density of states $\rho_0(\omega)$.

The results of numerical calculations carried out on the basis of the EHA method are presented in Figs 12–14. The first two figures give the Hubbard model results for the half-filled case. Fig. 12 shows how the density of states evolves for different values of the parameter U. At low values of U, particularly for $U = 0.5$, the function $\rho(\omega)$ differs little from a Gaussian curve centred at $\omega = 0$. As U increases, the peak $\rho(\omega)$ becomes deformed and shifts to the right, but in such a way that its amplitude [representing the density of states $\rho(\mu)$ at the Fermi level $\mu = U/2$] remains constant right up to $U = 2$.

The amplitude of the peak decreases in the range $U > 2$. A further increase in U results in the replacement of the peak with a dip and a bell-shape region, corresponding to the upper Hubbard subband, forming gradually to the right of the dip. The lower and upper Hubbard subbands move apart for $U > 4$. Therefore, variation of U induces the Fermi transition from the metal to the insulator state.

The inset in Fig. 12 gives the density of states $\rho(\mu)$ at the Fermi level as a function of U. In the range $2 < U < 4$ the system remains a metal, but its properties are very different from those of a Fermi liquid.

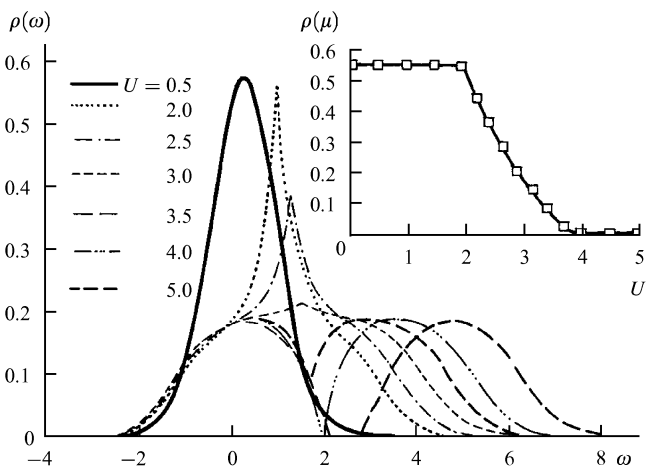

Figure 12. Density of states plotted, plotted as a function of ω for different values of U when $n = 1$, $T = 0$ [53]. The inset shows how the density of states on the Fermi surface depends on U.

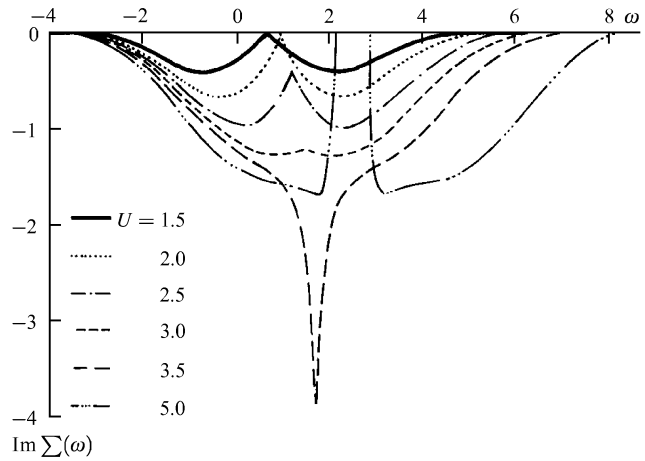

Figure 13. Imaginary part of the self-energy $\mathrm{Im}\,\Sigma(\omega)$, plotted for different values of U when $n = 1$ and $T = 0$ [53].

Calculations show that if $U > 2$, the imaginary part of the self-energy $\mathrm{Im}\,\Sigma(\omega)$ remains finite at the Fermi level, increases with increase in U, diverges as $U \approx 4$, and then vanishes (Fig. 13). Since in the Fermi-liquid case we can expect $\mathrm{Im}\,\Sigma(\omega) \propto (\omega - \mu)^2$ near the Fermi level, such behaviour implies breakdown of the Fermi-liquid picture. A calculation of the real part of the self-energy $\mathrm{Re}\,\Sigma(\omega)$ shows that for $U \approx 4$ the quasiparticle mass m^*/m diverges and an insulator gap appears at the Fermi level.

It follows that the EHA method predicts a continuous evolution from the metal phase to the insulator via an intermediate region of a non-Fermi-liquid metallic state. A comparison of the EHA results with the 'exact' calculations based on the quantum Monte Carlo method in the limit $d = \infty$ shows that the Edwards–Hertz approximate approach ensures a semiquantitative agreement in a wide range of parameters and temperatures.

Very interesting results are obtained by the EHA method limit when $n < 1$ (Fig. 14). Deviation from the half-filled case rapidly deforms the density of states $\rho(\omega)$ from its initial Gaussian profile to a double-peak shape, corresponding to two Hubbard subbands. When n is reduced, the density of states at the Fermi level reaches

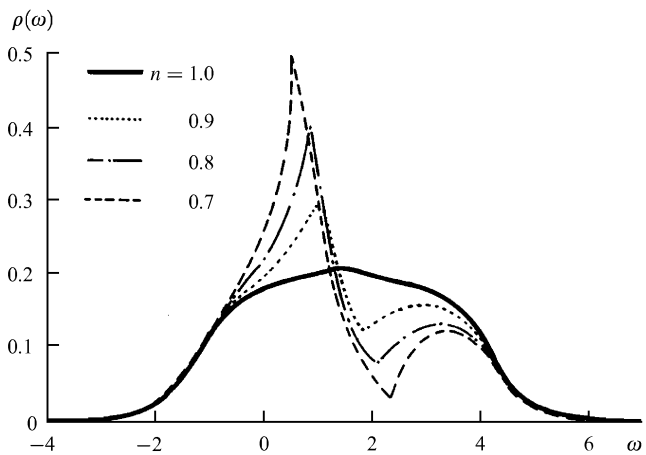

Figure 14. Density of states plotted for different values of n when $U = 3$ and $T = 0$ [53].

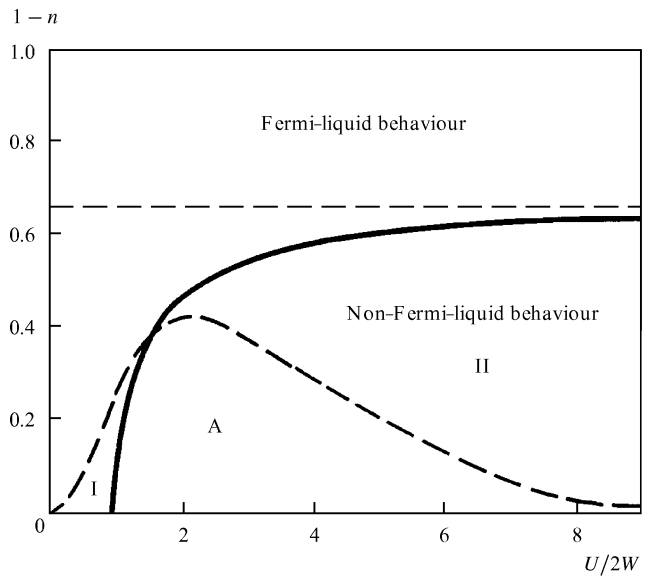

Figure 15. Phase diagram in the (U, n) plane obtained in the Hubbard model when $T = 0$ K [48].

values expected for an uncorrelated system and we again have Fermi-liquid behaviour. At high values of U this occurs at lower electron densities.

It therefore follows that at $T = 0$ we obtain a phase diagram shown in the (U, n) plane in Fig. 15. The continuous curve, calculated in the model of a semielliptic density of states [48], determines the region of Fermi-liquid behaviour of the system. The dashed curve in this figure represents the schematic boundary of the antiferromagnetic phase.

Magnetic ordering appears at $n = 1$ for all values of U. This implies complete nesting. In region I the antiferromagnetism appears in the Fermi-liquid phase. Region II corresponds to a disordered metallic (but not Fermi-liquid) phase. In the rest of the phase diagram the antiferromagnetism appears partly in the metal and partly in the insulator.

It is work noting the connection between two phenomena: the appearance of localised magnetic moments and non-Fermi-liquid behaviour. In the Fermi-liquid region there are no localised magnetic moments. They appear when $U \geqslant 2$, grow rapidly with increase in U, and give rise first to a non-Fermi-liquid metallic state and then (for $U \geqslant 4$) to an insulating state.

An attempt has recently been made to justify the EHA in terms of the standard diagram technique [50]. The main task has been to derive a functional $\Sigma[G]$, the existence of which would imply that this approximation is of the 'conserving' type [51, 52]. However, such a function has not been found and the problem of justification of the EHA method or of correcting it requires a separate investigation. Some aspects of the theory considered in the limit $d = \infty$ and a comparison with the perturbation theory results can be found in Refs [54–61].

4. Functional integration method

4.1 Static limit and the coherent potential approximation

The first successful theories of the magnetic behaviour of the Hubbard model in a wide range of the parameters U and n have been based on the representation of the

partition function Z by a functional integral and on the use of the static approximation [62–65]. The method is related to that described in Ref. [66], which is based on the single-impurity Anderson model [4]. This representation has been used in the preceding section for the single-site model.

In generalisation of Eqn (3.28) to a complete lattice the partition function Z can be represented by a functional integral in terms of η and ξ:

$$Z = Z_0 \int \delta\eta\, \delta\xi \exp\left\{-\frac{1}{2}\sum_{n=-\infty}^{\infty}(\xi_n^2+\eta_n^2) + \mathrm{Tr}\,\ln\left(1-G^0\hat{V}\right)\right\}. \tag{4.1}$$

Here, integration is carried out in terms of the fields of η_{in} and ξ_{in}, so that

$$\delta\eta\,\delta\xi = \prod_i \delta\eta_i\,\delta\xi_i\,,$$

$$\delta\eta_i = \mathrm{d}\eta_{i0}\prod_n \mathrm{d}^2\eta_{in}\,, \qquad \mathrm{d}^2\eta_{in} = \mathrm{d}(\mathrm{Re}\,\eta_{in})\,\mathrm{d}(\mathrm{Im}\,\eta_{in})$$

(and similarly for $\delta\xi_i$).

The trace in the argument of the exponential function in Eqn (4.1) applies to all the states which are characterised by an index representing the site, frequency, and spin; the operator $\hat{V}$ is diagonal; here,

$$V_{i\sigma} = \sqrt{\frac{U}{2\beta}}\,(\sigma\hat{\eta}_i + \hat{\xi}_i) \tag{4.2}$$

($\hat{\eta}_i$ and $\hat{\xi}_i$ are matrices of the frequency indices m and n) and Z_0 is the partition function for electrons in the absence of the interaction.

The problem of calculation of the partition function Z can be reduced in fact to calculation of the single-electron Green function $G = (1-G^0V)G^0$ in an arbitrary fluctuating external field (which is locally inhomogeneous and depends on time) and to averaging of the Gaussian distribution function over these fields.

In the static approximation, Eqn (4.1) is simplified by dropping from the trace all the components of the fields of η_{in} and ξ_{in}, except η_{i0} and ξ_{i0} corresponding to zero frequency (we shall denote the last two simply by η_i and ξ_i).

In the remaining functional integral the integration with respect to the charge fields ξ_i is carried out by the stationary phase method on the assumption that the frequencies of these fields are higher than fluctuations of the spin field. As a result, we obtain the partition function in the form of a functional integral with respect to the field η_i:

$$Z_{\mathrm{stat}} = Z_0 \int \prod_i \delta\eta_i \exp\left\{-\frac{1}{2}\sum_i \eta_i^2 + \mathrm{Tr}\,\ln\left(1-G^0\hat{V}\right)\right\}, \tag{4.3}$$

where $V'_{i\sigma} = \sqrt{U/2\beta}\,\sigma\eta_i$.

Application of the CPA to the quantity $1-G^0V'$ makes it possible to represent the functional integral (4.3) as a product of simple integrals, each applicable to a single site:

$$Z \approx Z_0 \prod_i \int_{-\infty}^{\infty} \delta\eta_i\, P(\eta_i)\,.$$

Here,

$$P(\eta_i) = \frac{1}{P}\exp\left\{-\frac{1}{2}\eta_i^2 + \sum_{\omega,n}\sum_{\sigma}\ln\left[\mathcal{G}_\sigma^{-1}(i\omega_n) - V'_{i\sigma}\right]\right\} \tag{4.4}$$

is the distribution function of the fields η_i.

In expression (4.4) the Green function $\mathcal{G}_\sigma$ represents the effective medium and in the CPA method it is found from expressions (3.19) and (3.21); P is the normalisation vector. The averages

$$\langle\eta\rangle \equiv \int \mathrm{d}\eta\, P(\eta)\,\eta\,, \qquad \langle\eta^2\rangle \equiv \int \mathrm{d}\eta\, P(\eta)\,\eta^2 \tag{4.5}$$

determine the spontaneous moment m and the localised moment at an atom $(\langle m^2\rangle)^{1/2}$.

Therefore, in the static approximation the problem reduces to calculation of the Green function $\mathcal{G}_\sigma$ by the CPA method and subsequent calculation of the field distribution function $P(\eta)$. This problem should be solved numerically. We shall see later that the static approximation links well the two limits: $U \gg W$ and $U \ll W$, i.e. the theory is in the nature of interpolation between the limit of localised magnetic moments and that of itinerant magnetism.

The static approximation works well at high temperatures, but gives rise to difficulties at low temperatures. For example, there are problems with a number of thermodynamic properties at $T=0$, since [64]

$$\left(\frac{\partial M}{\partial T}\right)_{T=0} = 0\,, \qquad (C_V)_{T=0} = 0\,, \qquad \left(\frac{\partial V}{\partial T}\right)_{T=0} = 0\,.$$

However, the above relationships are obeyed if the CPA method is replaced by the RPA [67].

The static approximation does not include spin-wave excitations and it overestimates the difference between the energies of the ferromagnetic and paramagnetic states [64] because correlations are ignored. This shortcoming can be avoided by including correlations with the aid of the Gutzwiller variational approach [2, 19]. This leads to the theory given in Ref. [64] in which the free energy at $T=0$ gives rise to a correlated ground state and which in the limit $T\to\infty$ yields results identical with those obtained in the static approximation.

4.2 Numerical calculation for the half-filled band case

Figs 16–18 give the results of calculations of the magnetic properties of the Hubbard model for a simple cubic lattice with the half-filled band ($n=1$). The calculations were carried out on the basis of the static approximation (dashed curves) and taking account of the dynamic corrections in the variational method (continuous curves). Different symbols are used in these figures to represent the results of a numerical calculation carried out for small clusters in accordance with the quantum Monte Carlo method. The ground state of the system for $n=1$ is a Neel antiferromagnet.

The sublattice magnetisation and the rms magnetic moment at a site are plotted as a function of the parameter U in Fig. 16. We can see that an increase in U increases the magnetisation from 0 to 1 (in terms of the Bohr magnetons) and goes over smoothly to a Heisenberg magnetic material with the atomic spin $S=1/2$ in the limit $U\to\infty$. The localised moment varies fastest in the range where $U\sim W$. The results obtained by the two calculation methods differ

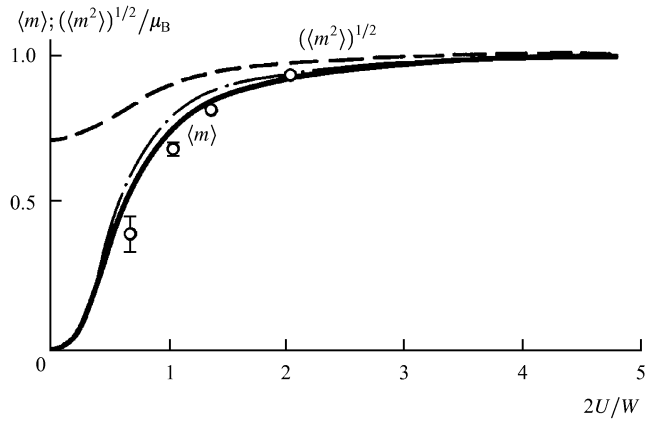

Figure 16. Sublattice magnetisation $\langle m\rangle$ and the localised moment $(\langle m^2\rangle)^{1/2}$ calculated in the Hubbard model for $n = 1$ and $T = 0$ [64]. The dashed curve represents the static approximation and the continuous curve includes the dynamic corrections [65]. The circles represent calculations carried out for small clusters [68].

only slightly and they are close to the results of calculations carried out for small clusters (represented by circles) [68]. In contrast to the magnetisation $\langle m\rangle$, the localised moment $(\langle m^2\rangle)^{1/2}$ depends weakly on U.

The next two figures give the temperature dependences of the magnetic properties. The phase diagram in the (T, U) plane is given in Fig. 17. A continuous or dashed curve separates the antiferromagnetic phase (A) from two paramagnetic phases: metal (PM) and insulator (PI). The curve separating the paramagnetic and antiferromagnetic phases is deduced from calculations of the Neel temperature for different values of $2U/W$ and the curve separating the metal and insulator phases is found from vanishing of the gap in the electron spectrum. This curve has not been calculated inside the antiferromagnetic phase region.

The dotted curves separate the boundaries of the antiferromagnetic phase deduced by the Hartree–Fock

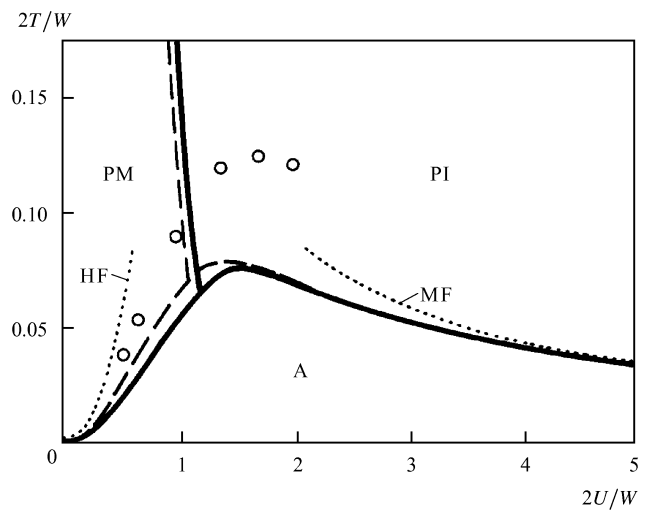

Figure 17. Phase diagram in the (T, U) plane, showing antiferromagnetic phase (A), the paramagnetic metal phase (PM), and the paramagnetic insulator phase (PI) [65]. The continuous and dashed curves have the same meaning as in Fig. 16; the dotted curves are explained in the text; the circles represent calculations for small clusters [69].

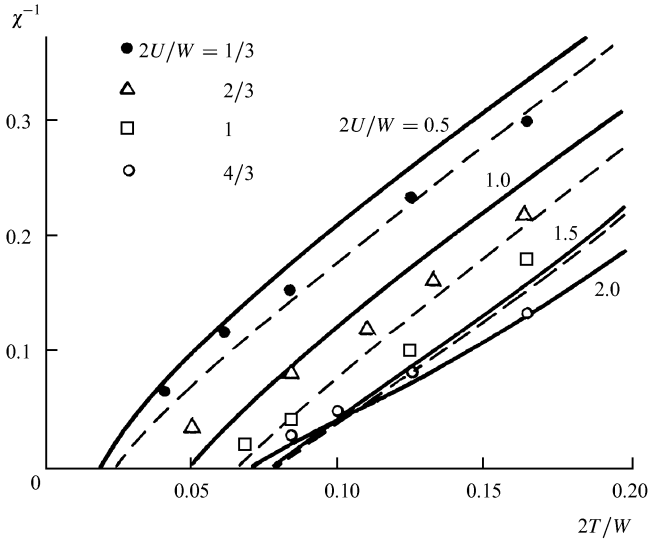

Figure 18. Temperature dependences of the reciprocal magnetic susceptibility of the antiferromagnetic phase, calculated for different values of $2U/W$ [65]. The continuous and dashed curves have the same meaning as in Fig. 16; points of different shapes are the results of calculations for small clusters [69].

(HF) approximation, for the case of low values $U \ll W$, and the molecular field (MF) approximation for the case of high values $U \gg W$. A continuous or dashed curve in Fig. 17 links these two limits. Therefore, the CPA theory is of the interpolation type. The large discrepancy between the results of this theory and those obtained by small-cluster calculations is attributed to the size effects [65].

The temperature dependence of the reciprocal magnetic susceptibility is linear in a wide range of temperatures. The Curie–Weiss behaviour of the susceptibility is evidence of the existence of localised magnetic moments, which depend weakly on temperature. This is confirmed by a direct calculation $(\langle m^2\rangle)^{1/2}$ for different values of T.

Fig. 18 gives the results calculated for different values of the parameter $2U/W$. In the limit of high U, these results agree with those obtained in the molecular field approximation, and for low values of U, they agree with the Hartree–Fock approximation. The magnetic behaviour of the model for $n = 1$ is evidently relatively insensitive to the bare density of states in the electron spectrum. For example, in the case of a semielliptic density of states the magnetic phase diagram remains the same as in Fig. 17 [70].

These results demonstrate that the simple theory relying on the static approximation and the CPA method is not very sensitive to the electron correlations. However, this conclusion may have to be modified greatly away from the half-filled band case, because the correlations can then be much more important.

5. Variational methods

5.1 Gutzwiller wave function

The variational methods are particularly effective in statistical physics problems, when regular perturbation theory cannot be used. A test wave function ψ_0 can be used to take account of the correlation effects in a purely intuitive manner and the ground-state energy can be found by varying the average energy

$$E = \frac{(\psi_0^* H \psi_0)}{(\psi_0^* \psi_0)} \tag{5.1}$$

over the free parameters that occur in ψ_0.

Gutzwiller had suggested [2] that, in the Hubbard model, ψ_0 should be selected in the form

$$\psi_0 = \prod_i \left[1 - (1-g) D_i\right] |0\rangle = g^D |0\rangle \ , \tag{5.2}$$

where $|0\rangle$ is the 'vacuum' wave function; $D_i = n_{i\uparrow} n_{i\downarrow}$, $D = \sum_i n_{i\uparrow} n_{i\downarrow}$, i.e. D is the electron-pair number operator for the lattice sites; $0 < g < 1$ is the variational parameter. A system of noninteracting electrons corresponds to $g = 1$. The value $g = 0$ corresponds to $U = \infty$ when all the states with a pair at each site are ignored.

It follows that the intermediate values of the variational parameter g correspond to states with the finite number of pairs in the system (which will be denoted by $N\bar{d}$). However, we can see from expression (5.2) that the probability of finding such states decreases rapidly with increase in their number (d is the average number of sites occupied by pairs).

The wave function (5.2) takes account globally of the reduction in the probability of occurrence of states with a large number of pairs. It has been found (see, for example, Ref. [71]) that such a simple method of including the correlation effects gives results, particularly in calculation of the ground-state energy.

The nature of the ground state determines selection of the 'vacuum' wave function in expression (5.2). In the case of the paramagnetic phase the function $|0\rangle$ is selected in the form of the 'Fermi-sea' wave function:

$$|0\rangle = \prod_{k\sigma} a_{k\sigma}^{\dagger} |\mathrm{vac}\rangle \ . \tag{5.3}$$

Here, $|\mathrm{vac}\rangle$ is the wave function of true vacuum.

If the symmetry of the ground state is broken, $|0\rangle$ is selected to be the wave function in the Hartree–Fock approximation. For example, for the antiferromagnetic state with the wave vector Q the 'vacuum' wave function is

$$|0\rangle = \prod_{k\sigma} \left[u_k a_{k\sigma}^{\dagger} + \sigma v_k a_{k+Q\sigma}^{\dagger}\right] |\mathrm{vac}\rangle \ , \tag{5.4}$$

where u_k and v_k are the well-known coefficients of the $u-v$ transformation.

We shall consider the paramagnetic ground state. The energy E_0 is the function of the average number $\bar{d}$ of pairs. It is represented by a sum of two terms: the potential energy $U\bar{d}$, which increases with increase in $\bar{d}$, and the kinetic energy which decreases with increase in $\bar{d}$. There is a certain optimal value of $\bar{d}$, found by differentiation of the average energy (5.1) with respect to the parameter $\bar{d}$. The variational parameter g is then related to $\bar{d}$ by [71]

$$g^2 = \frac{\bar{d}(1 - n_\uparrow - n_\downarrow + \bar{d})}{(n_\uparrow - \bar{d})(n_\downarrow - \bar{d})} \ . \tag{5.5}$$

In the paramagnetic phase the average number of electrons per site is $n_\uparrow = n_\downarrow = n/2$.

The values of $n_\uparrow$ and $n_\downarrow$ (or of the magnetisation $m = n_\uparrow - n_\downarrow$) should be found for the ferromagnetic phase by variation of the energy (5.1), together with the quantity $\bar{d}$. The energy of the antiferromagnetic ground state (5.4) should be varied in terms of the sublattice magnetisation m and the gap Δ in the electron spectrum, which occurs in the coefficients of the $u-v$ transformation. In this case the quantities g and $\bar{d}$ are linked by a relationship of the (5.5) type [72].

5.2 Gutzwiller approximation

Gutzwiller calculated the ground-state energy [19] with the aid of the wave function (5.1). The number of the spin configurations was found by a classical combinatorial method. This heuristic approach had no justification until it was shown that the Gutzwiller approximation corresponds exactly to calculation of the energy with the wave function (5.1) in the limit $d = \infty$ [72, 76]. We can thus see that one again the limit $d = \infty$ is important in determination of the relationship between the various approaches used in the SCES theory.

The results of calculations of the ground-state energy in the limit $d = \infty$ [72–76] will now be discussed briefly. The quantity $\langle \psi_0^* H \psi_0 \rangle$ was calculated by a diagram technique in terms of the parameter $1 - g^2$. This has proved to be the standard technique for the Green functions, but without account for the dynamics.

The perturbation-theory series can be expressed in terms of the zeroth-approximation functions:

$$P_{ij\sigma}^0 \equiv \langle \psi_0^* C_{i\sigma}^{\dagger} C_{j\sigma} \psi_0 \rangle \ . \tag{5.6}$$

In the case of high dimensions d of space the behaviour of the series (as functions of the distance between the sites) is determined by an asymptotic expression of the type (3.5). It then follows that in the limit $d = \infty$ the irreducible self-energy part is local, i.e.

$$S_{ij\sigma}^* = \delta_{ij} S_{ii\sigma}^* \ . \tag{5.7}$$

The sum of all the irreducible diagrams obtained in the limit $d = \infty$ can be expressed in terms of the exact correlation function $P_{ii\sigma}$:

$$S_{ii\sigma}^* = -\frac{1}{2P_{ii\sigma}} \left[1 - \sqrt{1 + 4(1-g^2) P_{ii\sigma} P_{ii,-\sigma}}\right] \ . \tag{5.8}$$

The matrices P_σ and P_σ^0 are then related by

$$P_\sigma = P_\sigma^0 + P_\sigma^0 S_\sigma P_\sigma^0 \ , \tag{5.9}$$

$$S_\sigma = \frac{1}{1 - S_\sigma^* P_\sigma} S^* \sigma \ . \tag{5.10}$$

In the case of a translationally invariant system the quantity $S_{ii\sigma}^* = S_\sigma^*$ is found from Eqns (5.8)–(5.10) and it can be expressed in terms of the average number (per site) n_σ of electrons with the spin σ:

$$S_\sigma^* = \frac{E_\sigma - \sqrt{E_\sigma^2 - 4(1-g^2)(1-n_\sigma) n_\sigma}}{2(1-n_\sigma)} \ , \tag{5.11}$$

where

$$E_\sigma = 1 - (1-g^2)(n_\sigma - n_{-\sigma}) \ .$$

Calculation of the average energy (5.1) gives

$$\frac{E}{N} = \sum_\sigma q_\sigma \bar{\varepsilon}_{0\sigma} + U\bar{d} \ . \tag{5.12}$$

Here,

$$q_\sigma = 1 - \frac{S_\sigma^*}{(1+g)^2} \left(1 - \frac{g^2}{1 - S_\sigma^*}\right) \ , \tag{5.13}$$

$$\bar{d} = \frac{g^2 n_\sigma}{1-g^2}\,\frac{S^*}{1-S^*}\,, \tag{5.14}$$

where $\bar{\varepsilon}_{0\sigma}$ is the kinetic energy (per one lattice site) of noninteracting electrons.

Expression (5.12), together with formulas (5.13) and (5.14), gives the energy of the investigated system as a function of the parameters $n_\uparrow$, $n_\downarrow$, and g. Minimisation in terms of these parameters can give the ground-state energy E_0.

In the Fourier space the quantity P_σ^0 represents the number $n_{k\sigma}^0$ of particles with the momentum k. Therefore, it follows from Eqn (5.10) that in the ground state the quantity S_σ is a discontinuous function of the momentum:

$$S_\sigma = \begin{cases} \dfrac{S_\sigma^*}{1-S_\sigma^*}\,, & k < k_{\mathrm{F}\sigma}\,, \\ S_\sigma^*\,, & k > k_{\mathrm{F}\sigma}\,. \end{cases} \tag{5.15}$$

Consequently, the distribution function of the particle momenta has a jump of the quantity q_σ at $k = k_{\mathrm{F}\sigma}$, which is given by formula (5.13). Therefore, in the limit $d = \infty$, the Hubbard model energy is expressed in terms of the average number of pairs and the jump of the momentum on the Fermi surface.

It is remarkable that expression (5.12) is identical with the result obtained in the Gutzwiller approximation, i.e. this approximation is exact in the limit $d = \infty$. In the general case (without assumption of translational invariance), we find that expression (5.12) becomes [74]

$$E = \sum_{i,j,\sigma} \sqrt{q_{i\sigma} q_{j\sigma}}\, P_{ij\sigma}^0 + U \sum_i \bar{d}_i\,, \tag{5.16}$$

which contains the local quantities d_i and $q_{i\sigma}$, given by formulas (5.14) and (5.13) with the local quantities $n_{i\sigma}$ and $S_{i\sigma}^*$. The theory can be generalised so as to yield corrections in the form of an expansion in the powers near the limit $d = \infty$ [76].

A calculation in accordance with the theoretical formulas gives, in the limit $d = \infty$, results which are in excellent agreement with those calculated for $d = 2$ by the quantum Monte Carlo method. The agreement is even better for $d = 3$. It is evident from Fig. 19 that even for $d = 2$ the corrections proportional to $1/d$ are very small, i.e. the Gutzwiller approximation gives a very accurate value of the ground-state energy and this energy is not very sensitive to the dimensionality d of space.

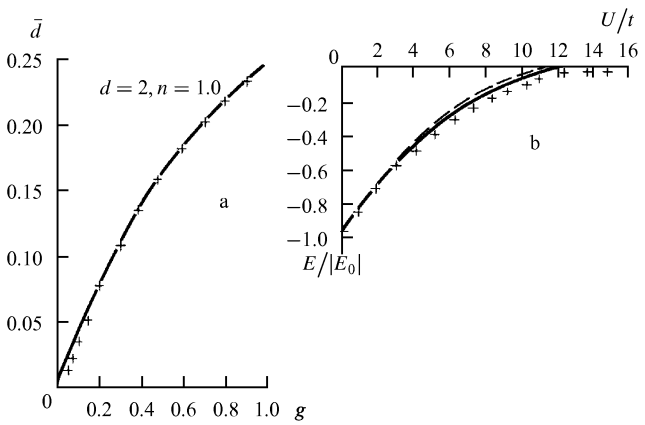

Figure 19. Comparison of the calculations, carried out in the Gutzwiller approximation (dashed curve) and taking account of the $1/d$ corrections (continuous curves), with the calculations carried out by the quantum Monte Carlo method (crosses) for: (a) the average number of pairs; (b) the ground-state energy in the two-dimensional Hubbard model [76].

A comparison of the energies of the paramagnetic, ferromagnetic, and antiferromagnetic phases makes it possible to construct the phase diagram in the (U, n) plane (Fig. 20). The dashed curves represent the boundaries of the phases deduced on the assumption that both magnetically ordered phases are homogeneous. If we assume the possibility of the existence of inhomogeneous phases, then these boundaries change to the continuous curves in Fig. 20.

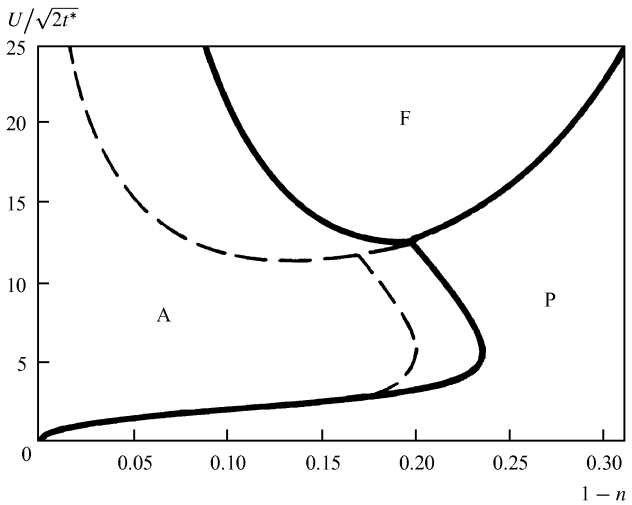

Figure 20. Magnetic phase diagram (continuous curves) at $T = 0$ K [77]. The dashed curves represent the phase diagram in which only the homogeneous states are considered.

It is found that the appearance of an antiferromagnetic phase with small ferromagnetic inclusions is favoured by energy considerations. The possibility of the appearance of such mixed phases has been studied in detail on the basis of the Hubbard model [78–82].

The magnetic phase diagram shown in Fig. 20 was determined [77] making use of the Gaussian density of states in the bare spectrum (3.4) corresponding to the limit $d = \infty$. Therefore, the quantity U in Fig. 20 is in units of t^*. Variational approaches have been used also in the investigations of the ferromagnetic state in the Hubbard model [83, 84].

6. Method of slave bosons and fermions

6.1 X operators

Under the conditions of a strong Coulomb interaction $(U \gg t)$ the Coulomb term can be used as the zeroth-approximation Hamiltonian. Since the interaction of electrons is considered in the Hubbard model for just one site, the zeroth-approximation problem reduces to the single-site problem and it can be solved exactly quite readily. In this situation it is convenient to use the basis

$$P\left(|i0\rangle,\ |i+\rangle,\ |i-\rangle,\ |i2\rangle\right) \tag{6.1}$$

of localised atomic functions at a site describing states free of electrons, those with one electron, and with an electron pair, respectively.

The transitions between various states are described by 4×4 matrices corresponding to the Hubbard X operators [85]

$$X_i^{pq} = |ip\rangle\langle iq| \ .$$

All the elements of such a matrix vanish, apart from one which is at the point of intersection of the pth row and the qth column, and which is equal to 1.

The transition from a state $|iq\rangle$ the a state $|ip\rangle$ can alter the number of electrons at a site by one or two, or it may leave this number unchanged. This means that some of the independent X^{pq} operators are Fermi-like (f operators) and some are Bose-like (b operators):

$$f(X^{0\sigma}, X^{\sigma 0}, X^{\sigma 2}, X^{2\sigma}), \quad b(X^{+-}, X^{-+}, X^{20}, X^{02}) \ , \tag{6.2}$$

whereas four operators are diagonal:

$$X^{00}, \ X^{++}, \ X^{--}, \ X^{22} \ .$$

Obviously, a product of two X operators is also an X operator or it vanishes in accordance with the rule

$$X^{rs}X^{pq} = \delta_{sp}X^{rq} \ . \tag{6.3}$$

The above rule can be used to form a commutator or an anticommutator of two X operators:

$$\left[X_i^{rs}, X_j^{pq}\right]_{\pm} = \delta_{ij}\left[\delta_{sp}X_i^{rq} \pm \delta_{rq}X_i^{ps}\right] \ . \tag{6.4}$$

It is understood that a commutator is used in the case of the b operators and an anticommutator for the f operators.

The X operators obey the following identity:

$$X_i^{00} + \sum_{\sigma} X_i^{\sigma\sigma} + X_i^{22} = 1 \ , \tag{6.5}$$

which represents completeness of the single-site states described by the basis (6.1). The X operators can be expressed in terms of the Fermi operators by the following relationships:

$$X_i^{00} = (1 - n_{i\uparrow})(1 - n_{i\downarrow}), \ X_i^{\sigma\sigma} = n_{i\sigma}(1 - n_{i-\sigma}) \ ,$$
$$X_i^{22} = n_{i\uparrow}n_{i\downarrow}, \ X_i^{\sigma 0} = a_{i\sigma}^{\dagger}(1 - n_{i-\sigma}), \ X_i^{2\sigma} = \sigma a_{i-\sigma}^{\dagger}n_{i\sigma} \ ,$$
$$X_i^{\sigma,-\sigma} = a_{i\sigma}^{\dagger}a_{i,-\sigma}, \ X_i^{20} = \sigma a_{i,-\sigma}^{\dagger}a_{i\sigma}^{\dagger} \ . \tag{6.6}$$

[The conjugate operators are found from the rule $(X^{pq})^{\dagger} = X^{qp}$.]

It follows from the relationships (6.6) that $X_i^{\sigma 0}$ and $X_i^{2\sigma}$ are Fermi-like operators. Their linear combination can be used to describe the Fermi operators themselves:

$$a_{i\sigma}^{\dagger} = X_i^{\sigma 0} + \sigma X_i^{2,-\sigma} \ . \tag{6.7}$$

The Hamiltonian (1.1) of the SCES model (including the chemical potential μ) expressed in terms of the X operators is

$$H = \sum_i \left\{-\mu X_i^{++} - \mu X_i^{--} + (U - 2\mu)X_i^{22}\right\}$$
$$+ t\sum_{i,j}\left\{(X_i^{+0} + X_i^{2-})(X_j^{0+} + X_j^{-2})\right.$$
$$\left. + (X_i^{-0} - X_i^{2+})(X_j^{0-} - X_j^{+2})\right\} \ . \tag{6.8}$$

It is remarkable that in this representation the Coulomb term, which is quartic in terms of the Fermi operators, becomes linear in the X operators and the kinetic energy becomes a quadratic form of these operators. All the advantages of the X operators follow from this linearisation of the Coulomb term.

The Hamiltonian (6.8) can be used to develop a regular theory of perturbations in powers of t/U in the form of a diagram technique for the X operators [24, 86]. This is described briefly in my earlier review [6] and we shall not deal with the subject here. Since the algebra of the X operators is fairly complex, the diagram technique involving them is far from simple, although it has certain advantages.

Here, other approaches will be considered and in these approaches the X operators are expressed in terms of products of the usual Fermi and Bose operators. Such representations comprise the technique of slave bosons and fermions, first presented in Refs [87, 88] for other models.

6.2 Boson and fermion representation of X operators

There are many different representations of this kind. They can be obtained making use of the following general relationship between the X_i^{pq} operators and the corresponding X^{pq} matrix:

$$X_i^{pq} = \psi_i^{\dagger}X^{pq}\psi_i \ , \tag{6.9}$$

where ψ_i is a four-component column composed of the Fermi and Bose annihilation operators.

Let us consider first the limiting case of the Hubbard model, which is the $t-J$ model in which only three states at a site are taken into account: $|i0\rangle$, $|i+\rangle$, $|i-\rangle$. Selecting ψ_i in the form

$$\psi_i^{\dagger} = (b_i^{\dagger}, f_{i\uparrow}^{\dagger}, f_{i\downarrow}^{\dagger}) \ ,$$

where $b_i^{\dagger}$ is a Bose operator and $f_{i\sigma}^{\dagger}$ is a Fermi operator, we find from the relationship (6.9) that

$$X_i^{0\sigma} = b_i^{\dagger}f_{i\sigma}, \quad X_i^{+-} = f_{i\uparrow}^{\dagger}f_{i\downarrow} \ , \tag{6.10}$$

which satisfies the transposition relationships for the X operators subject to the additional condition:

$$b_i^{\dagger}b_i + \sum_{\sigma} f_{i\sigma}^{\dagger}f_{i\sigma} = 1 \ . \tag{6.11}$$

This is known as the slave boson representation.

If ψ_i is selected in the form

$$\psi_i^{\dagger} = (f_i^{\dagger}, b_{i\uparrow}^{\dagger}, b_{i\downarrow}^{\dagger}) \ ,$$

the result is the slave fermion representation

$$X_i^{0\sigma} = f_i^{\dagger}b_{i\sigma}, \quad X_i^{+-} = b_{i\uparrow}^{\dagger}b_{i\downarrow} \tag{6.12}$$

subject to the additional condition

$$\sum_{\sigma} b_{i\sigma}^{\dagger}b_{i\sigma} + f_i^{\dagger}f_i = 1 \ . \tag{6.13}$$

In both cases a slave particle (boson or fermion) has no other index, apart from that identifying the site.

In the Hubbard model we can use, for example, the following representation in terms of slave bosons [89]:

$$X_i^{0\sigma} = e_i^{\dagger}f_{i\sigma}, \quad X_i^{00} = e_i^{\dagger}e_i \ ,$$
$$X_i^{2\sigma} = d_i^{\dagger}f_{i\sigma}, \quad X_i^{\sigma\sigma} = f_{i\sigma}^{\dagger}f_{i\sigma} \ , \tag{6.14}$$
$$X_i^{02} = e_i^{\dagger}d_i, \quad X_i^{22} = d_i^{\dagger}d_i$$

subject to the additional condition

$$e_i^\dagger e_i + d_i^\dagger d_i + \sum_\sigma f_{i\sigma}^\dagger f_{i\sigma} = 1 \ . \tag{6.15}$$

Here, the Bose operators $e_i^\dagger$ and $d_i^\dagger$ create states $|i0\rangle$ with an empty site and $|i2\rangle$ with a pair, and the Fermi operator $f_{i\sigma}^\dagger$ creates a state $|i\sigma\rangle$ with one electron per site:

$$|i0\rangle = e_i^\dagger|\mathrm{vac}\rangle \ , \quad |i\sigma\rangle = f_{i\sigma}^\dagger|\mathrm{vac}\rangle \ , \quad |i2\rangle = d_i^\dagger|\mathrm{vac}\rangle \ , \tag{6.16}$$

where $|\mathrm{vac}\rangle$ is the wave function of complete vacuum.

It is suggested in Ref. [90] that the basis functions can be written down with the aid of four slave bosons:

$$|i0\rangle = e_i^\dagger|\mathrm{vac}\rangle \ , \quad |i\sigma\rangle = f_{i\sigma}^\dagger p_{i\sigma}^\dagger|\mathrm{vac}\rangle \ , \quad |i2\rangle = f_{i\uparrow}^\dagger f_{i\downarrow}^\dagger d_i^\dagger|\mathrm{vac}\rangle \ . \tag{6.17}$$

This selection of the basis functions leads to a more complex (and not bilinear) X operator representation. The following conditions should then be satisfied to guarantee the absence of nonphysical states:

$$\begin{aligned} &e_i^\dagger e_i + \sum_\sigma p_{i\sigma}^\dagger p_{i\sigma} + d_i^\dagger d_i = 1 \ , \\ &f_{i\sigma}^\dagger f_{i\sigma} = p_{i\sigma}^\dagger p_{i\sigma} + d_i^\dagger d_i = 0 \ . \end{aligned} \tag{6.18}$$

The Hamiltonian (1.1) in the (6.17) representation is

$$H = t\sum_{i,j,\sigma} f_{i\sigma}^\dagger f_{i\sigma} Z_{i\sigma}^\dagger Z_{i\sigma} + U\sum_i d_i^\dagger d_i \ , \tag{6.19}$$

where

$$Z_{i\sigma} = e_i^\dagger p_{i\sigma} + p_{i,-\sigma}^\dagger d_i \ .$$

It follows that the Coulomb part of the Hamiltonian is diagonal, but all the difficulties are transferred to the kinetic part, which now has the form of the fermion–boson interaction. This situation is typical when different representations of the X operators are used, although the kinetic energy can assume a variety of forms.

There is an extensive literature on the use of the technique of slave bosons and fermions in the Hubbard and t–J models (see, for example, Refs [91–98]), particularly near the half-filled configuration. A comparison of the results obtained with the aid of slave bosons and fermions in the t–J model is made in Ref. [96]. There is no general prescription for selection of a specific representation.

6.3 Effect of constraints

When the X operators are expressed in terms of the fermion Bose operators, the problem is reduced to the methods of standard perturbation theory for the Fermi and Bose systems, but a new difficulty then arises: it is necessary to take account of additional conditions or constraints of the type described by representations of the (6.14) and (6.18) type, which remove nonphysical states, i.e. which return the extended Hilbert space to its initial state.

Constraints are usually taken into account by means of Lagrangian multipliers, which are used to write down the expressions for the partition function representing a functional integral in terms of the Fermi and Bose fields. For example, in the case of the Hamiltonian in the form (6.19) the integration with respect to the Grassman variables yields the following functional integral in terms of the Bose fields e_i, $p_{i\uparrow}$, $p_{i\downarrow}$, and d_i [90]:

$$Z = \int \delta e\, \delta p_\uparrow\, \delta p_\downarrow\, \delta d \prod_{i\sigma} \delta\lambda_i\, \delta\lambda'_{i\sigma}\, \exp\left[-\int_0^\beta \mathrm{d}\tau\, S(\tau)\right] \ , \tag{6.20}$$

where

$$\begin{aligned} S(\tau) = &\sum_i e_i^\dagger\left(\frac{\partial}{\partial\tau} + \lambda_i\right)e_i + \sum_{i,\sigma} p_{i\sigma}^\dagger\left(\frac{\partial}{\partial\tau} + \lambda_i - \lambda'_{i\sigma}\right)p_{i\sigma} \\ &+ \sum_i d_i^\dagger\left(\frac{\partial}{\partial\tau} + U + \lambda_i - \lambda'_{i\sigma}\right)d_i - \lambda_i \\ &+ \mathrm{Tr}\,\ln\left[\delta_{ij}\left(\frac{\partial}{\partial\tau} - \mu + \lambda'_{i\sigma}\right) + t_{ij}Z_{i\sigma}^\dagger Z_{j\sigma}\right] \ . \end{aligned} \tag{6.21}$$

Here, λ_i and $\lambda_{i\sigma}$ are the Lagrangian multipliers for the first and second equations in the system (6.18). The constraints of the system (6.18) are local and, therefore, λ_i and $\lambda_{i\sigma}$ depend on the site number i. However,they are independent of the second variable τ, because both constraints (6.18) commute with the Hamiltonian (6.19).

In work with the functional integral (6.20) the first approximation can be the saddle point approximation, in which it is assumed that the Bose fields and the Lagrangian multipliers are independent of the site and time. This implies the static approximation in terms of the Bose fields and the replacement of local constraints with global ones, i.e. those which are satisfied only on the average.

The static approximation leads to the following expression for the free energy $f = -kT\ln Z/N$:

$$\begin{aligned} f = Ud^2 - T\sum_\sigma \int \mathrm{d}\varepsilon\, \rho_0(\varepsilon)\ln\left\{1 + \exp\left[-\beta(q_\sigma\varepsilon - \mu + \lambda'_\sigma\right]\right\} \\ + \lambda\left(\sum_\sigma p_\sigma^2 + e^2 + d^2 - 1\right) - \sum_\sigma \lambda'_\sigma(p^2 + d^2) \ , \end{aligned} \tag{6.22}$$

where $q_\sigma = \langle Z_{i\sigma}^\dagger Z_{i\sigma}\rangle$. In the paramagnetic case when the band is half-filled ($n = 1$, $\mu = U/2$), minimisation with respect to λ and λ'_σ gives the free energy as a function of just one parameter d. At $T = 0$, we find that

$$f = 2q\int \mathrm{d}\varepsilon\, \rho_0(\varepsilon)\, \varepsilon f(q\varepsilon) + Ud^2 \ , \tag{6.23}$$

where

$$q = 8d^2(1 - 2d^2) \ . \tag{6.24}$$

The integral with respect to ε in Eqn (6.23) represents the average kinetic energy of electrons. Therefore, Eqn (6.23) is identical with expression (5.12) if the pair density $d^2 = \bar{d}$ is introduced. We thus obtain a remarkable result: the saddle point approximation in a functional integral representing the partition function in the Hubbard model with the aid of slave bosons at $T = 0$, equivalent to the Gutzwiller approximation known to be exact in the limit $d = \infty$.

Inclusion of the mean field fluctuations in a functional integral makes it possible to provide a theoretical treatment in which a strongly correlated system is described by boson and fermion fields coupled to one another by gauge fields, which take constraints into account [82, 92]. This approach has been used intensively in recent years in the study of the transport properties of SCES, the stimulus being provided by the anomalous behaviour of high-temperature superconductors in the normal metallic phase, particularly by the linear dependence of the electric resistance on T.

7. Main correlation effects

Several methods for investigating the Hubbard model in the strong correlation case ($U \geqslant W$) are described above. They should be supplemented by methods relying exclusively on computer calculations (high-temperature expansions, diagonalisation of small clusters), the results of which can be used to check approximate analytic approaches.

All the listed approaches (with the exception of the $d = \infty$ limit, which is discussed separately later) yield limited information on the physical properties of the main model in the SCES theory. A comparison of individual, frequently mosaic-like, results makes it possible to reconstruct the pattern of the most important correlation effects in the behaviour of the model.

7.1 Metal–insulator phase transition

The metal–insulator phase transition, predicted intuitively by Mott, was first confirmed by Hubbard over thirty years ago on the basis of the 'alloy analogy', i.e. in the spirit of the CPA method. Hubbard demonstrated that at some critical value $U_c \sim W$ a gap appears in the middle of a band in the initial electron spectrum, so that in the half-filled case the system becomes an insulator.

A consistent mean field theory, based on consideration of the limit $d = \infty$, shows that the pattern predicted by Hubbard is far too simplistic. In fact, in the half-filled case an increase in U gradually gives rise to a gap, but there is another effect: a sharp quasiparticle peak appears at the Fermi level and it corresponds to the Suhl–Anderson resonance due to the scattering of electrons by localised spin fluctuations. The effect of temperature on this peak is similar to that in the Kondo effect.

The existence of a sharp quasiparticle peak governs the transport properties of the system in the metallic phase. Under these conditions such behaviour of the Hubbard model corresponds to the behaviour of an effective single-impurity Anderson model to which the Hubbard model reduces in the limit $d = \infty$.

The latest investigations [105] show that the metal–insulator phase transition should be of the first order. Fig. 21 shows the Hubbard-model phase diagram obtained in the limit $d = \infty$ for the half-filled band case. This diagram is based on calculations carried out for a model density of states in the initial band described by a semicircle. This is known to correspond to the Bethe lattice in which each atom has z nearest neighbours which are in no way coupled to one another.

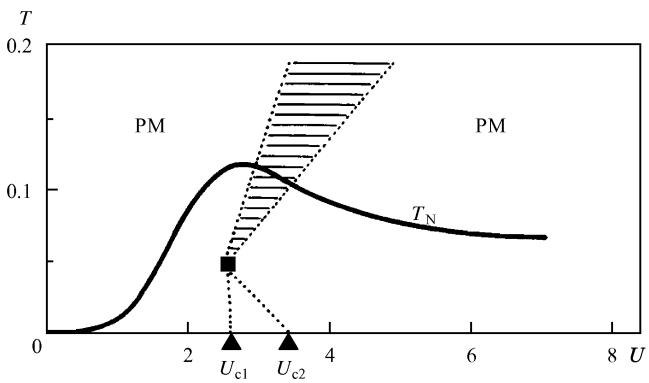

Figure 21. Phase diagram in the (T, U) plane calculated for the Bethe lattice on the assumption that $d = \infty$ and $n = 1$ [105].

In the case of the Bethe lattice it is possible to transform analytically the self-consistency equations (3.33)–(3.35) of the mean field theory. This simplifies greatly the subsequent numerical solution. As a result, the application of the quantum Monte Carlo method to the corresponding one-dimensional Anderson problem makes it possible to deal with lower temperatures.

It is found that at $T = 0$ the self-consistency equations have two different solutions, which coexist in the interval $U_{c1} < U < U_{c2}$. One of them corresponds to the metal phase and the other to the insulator phase; the points U_{c1} and U_{c2} correspond to the absolute loss of stability by the insulator and metal phases. At a finite temperature this interval becomes narrower and contracts to a point (represented by the square in Fig. 21).

Inside the triangle formed by the two dotted lines and the abscissa there is a line of the first-order phase transitions which is found by equating the energies of the metal and insulator phases. In the shaded regions (at higher temperatures) the two phases coexist and this makes possible a continuous crossover from one phase to the other. The boundaries of this region correspond to second-order phase transitions. The curve representing the antiferromagnetic phase transition lies above the metal–insulator phase transition line.

On the whole, the phase diagram shown in Fig. 21 resembles that predicted earlier [43] and shown in Fig. 11. Although the metal–insulator phase transition is well understood in the specific half-filled case, there are relatively few results for the more general case when the band is not half-filled.

7.2 Breakdown of the Fermi-liquid behaviour

The question of evolution of the nature of single-particle states of the metal phase has not yet been answered unambiguously. A complete pattern would identify the nature of the quasiparticle spectrum at each point in the three-dimensional space of the parameters (U, n, T). At present, we know only some sections formed by the (U, n) planes at $T = 0$ or by the (U, T) planes at $n = 1$. The majority of the results have been obtained in the mean field approximation ($d = \infty$).

Fig. 6 shows the change in the quasiparticle distribution function near the Fermi level in the half-filled case. An increase in U reduces continuously the jump at the Fermi level to zero, which is evidence of a continuous reduction in the amplitude Z of the coherent state and of the divergence of the effective mass m^*. However, the Fermi-liquid behaviour is retained right up to a certain critical value U_c, at which the insulator state appears as a result of a second-order phase transition.

The same conclusion follows from a qualitative analysis of the self-consistency equations [41] presented above. On the other hand, according to the Edwards–Hertz interpolation approach [48, 49], which is not based on the $d = \infty$ limit, the imaginary part of the quasiparticle self-energy does not vanish on the Fermi surface in a certain interval of the values of U, indicating breakdown of the Fermi-liquid behaviour in the metal phase (see Fig. 13).

A deviation from the half-filled band case reduces the region with the non-Fermi-liquid behaviour and the properties of the Fermi liquid are quite rapidly restored (Fig. 15). The problem of crossover from the Fermi-liquid behaviour to strong electron correlations in a metal as U is increased or as the half-filled band case is approached, is only outlined above and undoubtedly should be investigated further.

7.3 Crossover from itinerant magnetism to magnetism with localised magnetic moments

This problem has been discussed first in the literature in terms of localised spin fluctuations, starting from the weak coupling limit [9]. The next stage has been the use of the static approximation in the functional integration technique (Section 4 in this review).

Figs 16–18 show the pattern of the magnetic behaviour of the model in the half-filled band case, obtained in the static approximation by slow variation of $(\langle m^2\rangle)^{1/2}$ in Fig. 16 and by the Curie–Weiss contribution to the magnetic susceptibility (Fig. 18). It follows from Fig. 17 that the Neel temperature T_N, considered as a function of the Coulomb interaction U, has a minimum at $U \sim W$. The $T_N(U)$ curve links expressions (1.6) and (1.7) representing T_N in the weak and strong coupling limits.

The results of the static approximation are thus of interpolation nature. These results are supported qualitatively by a more rigorous approach corresponding to the $d=\infty$ limit in which the dynamics of the system is taken into account (Figs 7 and 8).

Two problems are the most pressing:

(1) How does the crossover from itinerant to localised magnetism occur when the electron density n is varied?

(2) How is the magnetic behaviour crossover related to the crossover of the electronic properties from the Fermi-liquid to the non-Fermi-liquid behaviour?

A clear solution has not yet been obtained to either of the problems. In the first case this is because the attention of researchers has been concentrated mainly on the behaviour of the model near the half-filled state (in connection with the problem of high-temperature superconductors).

The second problem is intrinsically complex and investigations of the quasiparticle spectrum model itself have just begun. One of the latest results is the phase diagram presented in Fig. 15. Phase diagrams of this type should be supplemented by identifying the regions where the magnetic-behaviour crossover takes place.

An attempt has been made to establish the magnetic crossover when the electron density is varied and to discover the relationship between the magnetic and electron crossovers in the limit of strong electron correlation $(U \gg W)$ within the framework of the $t-J$ model [11–13].

8. Conclusions

The overall conclusion of this review can be stated as follows. The $d=\infty$ limit provides the most universal and effective method for investigating the Hubbard model. It makes it possible to formulate the mean field approximation for strongly interacting fermions, which is correct from the point of view of requirements of statistical mechanics.

The main equations in this approximation yield the correct results in the limits $U \ll W$ and $U \gg W$. These equations are valid for any values of the parameters U, W, and the electron density n. In the $d=\infty$ limit the statistical mechanics of the Hubbard model on a lattice reduces to the statistical mechanics of an auxiliary single-impurity Anderson model (with specially selected parameters), which has well-known solutions.

In the $d=\infty$ limit the Hubbard model describes the most important among the correlation effects: the metal–insulator transition, the crossover from itinerant magnetism to localised magnetic moments, the breakdown of the Fermi-liquid behaviour near the boundaries of the metal–insulator phase transition.

In a comparison of the results of the theory in the limit $d=\infty$ with numerical calculations, carried out for $d=3$ and $d=2$ by the quantum Monte Carlo method or by the method of exact diagonalisation of small clusters, it was demonstrated that in many cases the agreement between the results is not only qualitative, but even quantitative. Naturally, the $d=\infty$ limit, corresponding to the mean field approximation, cannot describe the dynamics of fluctuations such as spin waves in a magnetically ordered phase. However, there are ways for including corrections of the order of $1/d$, which make it possible to solve problems of this kind.

Unfortunately, in the $d=\infty$ limit the mean field theory deals with consistency equations requiring a large volume of computer calculations. Further investigations of this type should be accompanied by development of approximate analytic methods for solving these equations, which need to be only qualitative. A recent paper [106] reports an investigation of this type.

The $d=\infty$ limit has been used also in other models employed in the theory of strongly correlated systems, for example, in the $t-J$ model [107, 108], in the Anderson lattice [109], and in the extended Hubbard models [11, 110, 112]. It has recently been applied to models with disorder. For example, interference of the effects of the strong Coulomb interaction and of disorder in the metal–insulator phase transition, i.e. the relationship between the Mott and Anderson electron localisation mechanisms, has been studied in the Hubbard model with disorder.

Introduction of the $d=\infty$ limit into the theory of strongly correlated systems has given a new impetus to the physics of this system. The situation now resembles the familiar state twenty years ago, when the important role of the $d=4$ dimensionality in the theory of second-order phase transitions has become understood and the ε expansion has been proposed, providing a universal method for investigating systems with strongly interacting fluctuations.

References

1. Hubbard J *Proc. R. Soc. London Ser. A* **276** 238 (1963)
2. Gutzwiller M C *Phys. Rev. Lett.* **10** 159 (1963)
3. Kanamori J *Prog. Theor. Phys.* **30** 275 (1963)
4. Anderson P W *Phys. Rev.* **124** 41 (1961)
5. Shubin S P, Wonsowsky S V *Proc. R. Soc. London Ser. A* **145** 159 (1934)
6. Izyumov Yu A *Usp. Fiz. Nauk* **161** (11) 1 (1991) [*Sov. Phys. Usp.* **34** 935 (1991)]
7. Izuyama T, Kim D, Kubo R *J. Phys. Soc. Jpn.* **18** 1025 (1963)
8. Penn D R *Phys. Rev.* **142** 350 (1966)
9. Moriya R *Spin Fluctuations in Itinerant Electron Magnetism* (Berlin: Springer, 1985)

10. Chao K A, Spalek J, Oles A M *J. Phys.C* **10** L271 (1977)
11. Izyumov Yu A, Letfulov B M *J. Phys. Condens. Matter* **2** 8905 (1990)
12. Izyumov Yu A, Letfulov B M, Shipitsyn E V *J. Phys. Condens. Matter* **4** 9951 (1992)
13. Izyumov Yu A, Letfulov B M, Shipitsin E V *Zh. Eksp. Teor. Fiz.* **105** 1357 (1994) [*J. Exp. Theor. Phys.* **78** 731 (1994)]
14. Hubbard J *Proc. R. Soc. London Ser. A* **281** 401 (1964)
15. Mott N F *Philos. Mag.* **6** 287 (1961)
16. Metzner W, Vollhardt D *Phys. Rev. Lett.* **62** 324 (1989)
17. Hubbard J *Phys. Rev. B* **19** 2626 (1979); **20** 4584 (1979); **23** 5974 (1981)
18. Hasegawa H *J. Phys. Soc. Jpn.* **46** 1504 (1979); **49** 178 (1980)
19. Gutzwiller M C *Phys. Rev. A* **137** 1726 (1965)
20. Bogolyubov N N, Tyablikov S V *Dokl. Akad. Nauk SSSR* **126** 53 (1959) [*Sov. Phys. Dokl.* **4** 589 (1959)]
21. Zubarev D N *Usp. Fiz. Nauk* **71** 71 (1960) [*Sov. Phys. Usp.* **3** 320 (1960)]
22. Zaitsev R O *Zh. Eksp. Teor. Fix.* **70** 1100 (1976); **75** 2362 (1978) [*Sov. Phys. JETP* **43** 574 (1976); **48** 1193 (1978)]
23. Goryachev E G, Kuzmin E V, Ovchinnikov S G *J. Phys. C* **15** 1481 (1982)
24. Izyumov Yu A, Skryabin Yu N *Statisticheskaya Mekhanika Magnitouporyadochennykh Sistem* (Statistical Mechanics of Magnetically Ordered Systems) (Moscow: Nauka, 1987)
25. Ehrenreich H, Schwartz L M *Solid State Phys.* **31** 150 (1976)
26. Arai T, Cohen M H *Phys. Rev. B* **15** 1836 (1977); **21** 3300, 3309 (1980)
27. Anokhin A O, Irkhin V Yu *Phys. Status Solidi B* **165** 129 (1991)
28. Anokhin A O, Irkhin V Yu, Katsnelson M I *J. Phys.Condens. Matter* **3** 1475 (1991)
29. Muller-Hartmann E *Solid State Commun.* **12** 1269 (1973)
30. Muller-Hartmann E *Z. Phys. B* **76** 211 (1989)
31. Brandt U, Meilsch C *Z. Phys. B* **75** 365 (1989); **79** 295 (1990)
32. Velicky B, Kirkpatrick S, Ehrenreich H *Phys. Rev.* **175** 747 (1968)
33. Vollhardt D, in *Proceedings of International School of Physics 'Enrico Fermi', Course 121* (Eds R A Broglia, J R Schrieffer) (Amsterdam: North-Holland, 1994) p. 31
34. Georges A, Kotliar G *Phys. Rev. B* **45** 6479 (1992)
35. Jarrell M *Phys. Rev. Lett.* **69** 168 (1992)
36. Janis V, Vollhardt D *Int. J. Mod. Phys. B* **6** 731 (1992)
37. Wolff P A *Phys. Rev.* **124** 1030 (1961)
38. Haldane F D M *Phys. Rev. Lett.* **40** 416 (1978)
39. Georges A, Kotliar G, Si Q *Int. J. Mod. Phys. B* **6** 705 (1992)
40. Georges A, Krauth W *Phys. Rev. Lett.* **69** 1240 (1992)
41. Rozenberg M J, Zhang X Y, Kotliar G *Phys. Rev. Lett.* **69** 1236 (1992)
42. Zhang X Y, Rozenberg M J, Kotliar G *Phys. Rev. Lett.* **70** 1666 (1993)
43. Pruschke T, Cox D L, Jarrell M *Phys. Rev. B* **47** 3553 (1993)
44. Jarrell M, Pruschke T *Z. Phys. B* **90** 187 (1993)
45. Scalettar R T, Scalapino D J, Sugar R L, Toussaint D *Phys. Rev. B* **39** 4711 (1989)
46. Leib E H, Wu F Y *Phys. Rev. Lett.* **20** 1445 (1968)
47. Frahm H, Korepin V E *Phys. Rev. B* **42** 10553 (1990)
48. Edwards D M, Hertz J A *Physica B* **163** 527 (1990)
49. Wermbter S, Czycholl G *J. Phys. Condens. Matter* **6** 5439 (1994)
50. Edwards D M *J. Phys. Condens. Matter* **5** 161 (1993)
51. Baym G, Kadanoff L P *Phys. Rev.* **124** 287 (1961)
52. Baym G *Phys. Rev.* **127** 1391 (1962)
53. Schweitzer H, Czycholl G *Z. Phys. B* **79** 377 (1990)
54. Janis V *Z. Phys. B* **83** 227 (1991)
55. van Dongen P G J *Phys. Rev. Lett.* **67** 757 (1991)
56. van Dongen P G J, Vollhardt D *Phys. Rev. Lett.* **65** 1663 (1990)
57. Ohkawa F J *J. Phys. Soc. Jpn.* **61** 1615 (1992)
58. Dobrosavljevic V, Kotliar G *Phys. Rev. B* **50** 1430 (1994)
59. Hirsch J E, Fye R M *Phys. Rev. Lett.* **56** 2521 (1986)
60. Zlatic V, Horvatic B *Phys. Rev. B* **28** 6904 (1983)
61. Menge B, Muller-Hartmann E *Z. Phys. B* **82** 237 (1991)
62. Cyrot M *J. Phys.* (Paris) **33** 125 (1972)
63. Takahashi Y *J. Phys. Soc. Jpn.* **55** 3553 (1986)
64. Kakehashi Y, Fulde P *Phys. Rev. B* **32** 1595 (1985)
65. Kakehashi Y, Hasegawa H *Phys. Rev. B* **37** 7777 (1988)
66. Schrieffer J R, Evenson W E, Wang S Q *J. Phys. (Paris)* **32** C1 (1971)
67. Hertz J A, Klenin M A *Phys. Rev. B* **10** 1084 (1974)
68. Yokoyama H, Shiba H *J. Phys. Soc. Jpn.* **56** 3582 (1987)
69. Hirsch J E *Phys. Rev. B* **35** 1851 (1987)
70. Kakehashi Y, Samson J H *Phys. Rev. B* **33** 298 (1986)
71. Vollhardt D *Rev. Mod. Phys.* **56** 99 (1984)
72. Metzner W, Vollhardt D *Phys. Rev. Lett.* **62** 324 (1989)
73. Metzner W *Z. Phys. B* **77** 253 (1989)
74. Vollhardt D, van Dongen P G J, Gebhard F, Metzner W *Mod. Phys. Lett.* **4** 499 (1990)
75. van Dongen P G J, Gebhard F, Vollhardt D *Z. Phys. B* **76** 199 (1989)
76. Gebhard F *Phys. Rev. B* **41** 9452 (1990)
77. Fazekas P, Menge B, Muller-Hartmann E *Z. Phys. B* **78** 69 (1990)
78. Nagaev E L *Physics of Magnetic Semiconductors* (Moscow: Mir, 1983)
79. Visscher P B *Phys. Rev. B* **10** 943 (1974)
80. Ogawa T, Kanda K, Matsubara K *Prog. Theor. Phys.* **53** 614 (1975)
81. Florencio J Jr, Chao K A *Phys. Rev. B* **14** 3121 (1976)
82. Ioffe L B, Larkin A I *Phys. Rev. B* **39** 8988 (1989)
83. Shastry B S, Krishnamurthy H R, Anderson P W *Phys. Rev. B* **41** 2375 (1990)
84. van der Linden W, Edwards D M *J. Phys. Condens. Matter* **3** 4917 (1991)
85. Hubbard J *Proc. R. Soc. London Ser. A* **285** 542 (1965); **296** 82 (1966)
86. Zaitsev R O *Zh. Eksp. Teor. Fiz.* **68** 207 (1975); **70** 1100 (1976) [*Sov. Phys. JETP* **41** 100 (1975); **43** 574 (1976)]
87. Barnes S E *J. Phys. F* **6** 1375 (1976)
88. Coleman P *Phys. Rev. B* **29** 3035 (1984)
89. Zou Z, Anderson P W *Phys. Rev. B* **37** 627 (1988)
90. Kotliar G, Ruckenstein A E *Phys. Rev. Lett.* **57** 1362 (1986)
91. Kane C L, Lett P A, Read N *Phys. Rev. B* **39** 6880 (1989)
92. Nagaosa N, Lee P A *Phys. Rev. Lett.* **64** 2450 (1990); Lee P A, Nagaosa N *Phys. Rev. B* **46** 5621 (1992)
93. Fresard R, Wolfle P *Int. J. Mod. Phys. B* **6** 685 (1992)
94. Grilli M, Kotliar G *Phys. Rev. Lett.* **64** 1170 (1990)
95. Arovas D P, Auerbach A *Phys. Rev. B* **38** 316 (1988)
96. Feng S, Wu J B, Su Z B, Yu L *Phys. Rev. B* **47** 15192 (1993)
97. Tanamoto T, Kuboki K, Fukuyama H *J. Phys. Soc. Jpn.* **60** 3072 (1991)
98. Markelov A V *Mod. Phys. Lett. B* **6** 1181 (1992)
99. Khaliullin G G *Pis'ma Zh. Eksp. Teor. Fiz.* **52** 999 (1990) [*JETP Lett.* **52** 389 (1990)]
100. Wang Y R, Rice M J *Phys. Rev. B* **49** 4360 (1994)
101. van Dongen P G J, Janis V *Phys. Rev. Lett.* **72** 3258 (1994)
102. Janis V *Phys. Rev. B* **49** 1612 (1994)
103. Jarrell M, Pruschke T *Phys. Rev. B* **49** 1458 (1994)
104. Zhang X Y, Zhang G M *Phys. Rev. B* **49** 7929 (1994)
105. Rozenberg M J, Kotliar G, Zhang X Y *Phys. Rev. B* **49** 10181 (1994)
106. Li Y M, d'Anbrumenil N *Phys. Rev. B* **49** 6058 (1994)
107. Metzner W, Schmit P, Vollhardt D *Phys. Rev. B* **45** 2237 (1992)
108. Strack R, Vollhardt D *Phys. Rev. B* **46** 13852 (1992)
109. Czycholl G, Schweitzer H *Phys. Scr.* **T-45** 125 (1992)
110. van Dongen P G J *Phys. Rev. Lett.* **67** 757 (1991)
111. Si Q, Kotliar G *Phys. Rev. B* **48** 13881 (1993)
112. Si Q, Kotliar G *Phys. Rev. Lett.* **70** 3143 (1993)